HEAT TRANSFER AND PRESSURE INVESTIGATIONS OF AN SI/S-IV STAGE SEPARATION MODEL USING SHORT-DURATION TECHNIQUES

Volume I: Introduction and General Method

By: C.L. Matthis

Contract No. NAS8-823

CAL Report No. HM-1510-Y-11

June 1964

CORNELL AERONAUTICAL LABORATORY, INC.

OF CORNELL UNIVERSITY, BUFFALO 21, N. Y.

CORNELL AERONAUTICAL LABORATORY, INC.
BUFFALO 21, NEW YORK

CAL REPORT NO. HM-1510-Y-11

HEAT TRANSFER AND PRESSURE INVESTIGATIONS OF AN SI/S-IV STAGE SEPARATION MODEL USING SHORT-DURATION TECHNIQUES

Volume I: Introduction and General Method

CONTRACT NO. NAS 8-823

JUNE 1964

BY C.L. Matthis /1149
C.L. Matthis

APPROVED K. C. Hendershot DATE Aug. 10, 1964
K.C. Hendershot, Head
Propulsion Section

APPROVED K. D. Bird DATE Aug. 10, 1964
K.D. Bird, Head
Applied Hypersonic Research Dept.

TABLE OF CONTENTS

TABLE OF CONTENTS (Cont'd)

LIST OF TABLES - VOLUME I

VOLUME II

LIST OF FIGURES - VOLUME I

LIST OF FIGURES - VOLUME I (Cont'd)

APPENDIX A

VOLUME II

LIST OF FIGURES - VOLUME II (Cont'd)

FOREWORD

This report was prepared by Cornell Aeronautical Laboratory, Inc. as part of a continuing research program conducted under Contract NAS 8-823, "Research Relative to the Application of Shock-Tube Techniques to the Study of Rocket Motor Vehicles." The program is administered under the direction of the Aeroballistics Division of the George C. Marshall Space Flight Center with Mr. H. B. Wilson, Jr. as the technical supervisor.

The over-all CAL program began in December 1960 with base heating investigations of a four-engine S-IV stage configuration followed by similar studies on the six-engine S-IV stage. The program described herein is a continuation of the S-IV base heating program through stage separation. Since the Douglas Aircraft Company is the prime contractor for the S-IV stage, necessary configuration information and test program requirements were supplied to CAL by Douglas. Mssrs. J. A. Tobias and L. Mouser of the Douglas Aircraft Company served as technical representatives during the program.

The author wishes to acknowledge the contributions of the colleagues in the CAL Applied Hypersonic Research Department, namely: T. J. Bell and M. Urso for their invaluable help in the conduct of the experimental program and in the solving of instrumentation difficulties and L. Swiatkowski and C. Britt for their assistance in the reduction and tabulation of the large amount of data obtained during the program.

ABSTRACT

An application of the short duration technique for simulating liquid propellant rockets is described. The project described is the high altitude investigation of the heat transfer and pressure environment encountered in the interstage region during a "fire-in-the-hole" separation of the S-IV second stage and the S-I first stage of the Saturn I launch vehicle.

The S-IV stage propulsion system utilizes a cluster of six RL 10-A3 liquid hydrogen/liquid oxygen rocket engines. Among the parameters investigated in this 1/10 scale model simulation program were: interstage vent size and shape, location and number of vents, stage separation distance, separation plane, engine gimballing and engine out, one vent panel not out, blast deflector configuration, heat shield shroud configuration, ambient altitude, and rocket engine chamber pressure and O/F ratio.

This report has been prepared in two volumes the first of which contains an introduction to the problem, the general method of experimentation, and a summary of the results. Volume II contains detailed tabulations of the numerical data only. No detailed analysis of the data is included in either volume, nor is any attempt made to extrapolate data to a full scale flight vehicle.

SECTION I INTRODUCTION

Rocket vehicle configurations characteristic of the various space boosters in use today employ engines in which the nozzle flows are normally under-expanded at high altitudes; hence a large amount of plume expansion occurs outside of the rocket exhaust nozzles creating heating problems due to exhaust jet interaction and resultant reverse flow into the base region.[1] If the engines of an upper stage of a multistage vehicle are ignited before the vehicle stages separate, the flow patterns arising from this fire-in-the-hole technique compound the heating problems as a result of additional recirculation induced in the interstage area and even more severe heating conditions may be encountered. On a typical multistage vehicle, the following areas may be affected by these adverse conditions; first stage bulkhead, second stage heat shield and thrust structure, first/second interstage walls, and any control packages, instrumentation, or miscellaneous auxiliaries located in this area.

The purpose of the model test program described herein was to acquire a detailed knowledge of the gas dynamic processes involved in the fire-in-the-hole staging sequence for the S-I/S-IV booster and to study the effects of various parameteric changes.

Short duration flow techniques similar to those used in shock tunnel testing have been developed at CAL for application to the experimental study of base heating.[2] These techniques are based on the concept that rocket flows need be duplicated only for that length of time sufficient to establish steady flow patterns and make the desired measurements. Rocket engine flows of the proper compositions and thermodynamic properties lasting a few milliseconds are generated. It has been shown in Reference 2 that this technique provides a sufficient period for flow establishment. Heat transfer and pressure measurements[3, 4] are made with fast-response instrumentation that has been developed for shock tunnel testing.

As reported in Reference 2, base heating investigations using the short-duration techniques were made on the earlier 4-engine Saturn S-IV configuration. With the modification of the S-IV from 4 to 6 engines, a program was initiated by NASA at CAL to provide design data for this 6-engine cluster configuration. This work has been reported in Reference 5 and the present stage-separation program is a continuation of that effort.

SECTION II TEST EQUIPMENT

A. Combustor

A short-duration constant-pressure combustor using gaseous oxygen and hydrogen was employed to generate the required products of combustion. A schematic drawing of this combustor and its propellant supply system wave diagram are shown in Figure 1. Reference 6 gives a more complete and detailed description of the combustor and its operating characteristics.

Briefly, the combustor operates as follows. Separate propellant supply tubes, sealed at the downstream ends with mylar diaphragms, are charged with gaseous hydrogen and oxygen. When the diaphragms are cut, flow commences out of the tubes, through an injector and into the combustion chamber. The combustion chamber is common to all six engines of the model. The engines contain diaphragms in the nozzle throats prohibiting the burned gases from flowing out of the nozzles until the desired combustion pressure has been attained. The combustion chamber is initially evacuated so that compression heating in the starting process will normally cause the mixture to autoignite. A spark plug is used as a backup ignition source so that if for any reason the mixture should fail to autoignite at the proper pressure, it will be caused to ignite by the spark before high pressures can build up which may lead to destructive over-pressure conditions.

The period of steady combustion is determined by the time required for the expansion waves created by the diaphragm opening to travel the lengths of the charge tubes and return to the combustion chamber as shown in Figure 1. Normally, the test time is not limited by the time of steady combustion but rather by the reflection of a blast wave which originates from the bursting of the nozzle diaphragms and reflects from the vacuum chamber walls. Although the effects of this reflected blast wave on the pressure and heat transfer on unconfined bases may be small, they are in general not negligible. However, in a confined environment such as the S-I/S-IV interstage region where heat fluxes and pressures are at least an order of magnitude higher than in the unconfined case, this effect is negligible. Hence, in order to provide adequate

SECTION II (Cont'd) TEST EQUIPMENT

time for the interstage to fill and reach equilibrium, the normal lengths of the propellant supply tubes were increased to provide approximately 10 milliseconds of steady combustion, or approximately twice the normally required test time. The propellant flow rates from the tubes necessary to maintain the proper combustion pressure and oxygen/fuel ratio are controlled by properly sized sharp-edge orifice plates located just upstream of the diagram stations. A typical combustion pressure record is shown in Figure 2C. It may be noted that the combustion pressure rises smoothly to a steady level in about 3-4 milliseconds. At this time the nozzle diaphragms open and nearly constant pressure is maintained for 9-10 milliseconds.

B. Model and Test Chamber Installation

The model used for these tests is a 1/10 scale model of the six-engine Saturn S-IV base region and adjoining interstage. The model of the base region used for previous CAL base heating studies[5] was used for the separation study with only minor modifications. Essentially, the model consists of a combustion chamber, six nozzles, a heat shield, an interstage extension with blast deflectors, and heat transfer and pressure instrumentation. Details of the model configuration are shown in Figures 3 through 7 which are reproduced from References 7 and 8.

The combustion or plenum chamber has been described in the previous section and serves the purpose of burning the gaseous propellants and directing the flow equally to the six nozzles.

The nozzles are set at a nominal 6 degree outward cant angle. All nozzles have the capability of being gimballed as shown in Figure 8.

The heat shield configuration was modified somewhat from the original S-IV 6 engine base heating model, being hexagonal rather than round as in the previous S-IV tests.

The interstage section is composed of four subsections: the basic interstage used throughout the test; the variable length stage providing four variable

lengths for the model; the vent area extension which permits changing vent area, shape and location; and the blast deflectors which provide different flow paths for the exhaust gases out through the interstage vents.

A second minor variation from the original S-IV configuration involved the placement of a conical section concentric with the port housing (plenum chamber) to simulate the Saturn S-IV thrust structure surface as shown in Figure 4.

The model is assembled directly to the aft end of the combustor and then inserted through a port in the end of the altitude chamber. A bulkhead provides for attachment of the combustor to the chamber and forms a vacuum seal.

Since at the high altitudes of interest the effect of the external flow is negligible, altitude simulation is achieved by duplicating the ambient pressure only. The altitude-simulation chamber is approximately 13 feet in diameter by 15 feet long. An altitude simulation capability up to 260,000 feet (10 microns Hg) is provided by a mechanical vacuum pump. The ambient pressure altitude remains essentially constant until the disturbance caused by the rocket firing is reflected back from the tank walls to the model region.

Model interstage positioning is provided by a support sting fastened to the blast deflector. This shaft, supported by tie rods to the test chamber, is moveable and can be accurately located through the aid of a rack and pinion drive between the shaft and support system. A sketch showing the relative positions of the S-IV stage and the interstage during the separation sequence is shown in Figure 9. Figure 10 describes the various interstage configurations while a schematic of the model, test chamber, and support system is shown in Figure 11.

C. Instrumentation

The thrust structure, heat shield, blast deflectors, and interstage extensions were instrumented with heat transfer and pressure instrumentation for detection and quantitative measurement of the complex flow phenomena

SECTION II (Cont'd) TEST EQUIPMENT

associated with fire-in-the-hole operation. This instrumentation, developed at CAL to meet the particular requirements of short-duration testing, is described in detail in References 3, 4 and 9.

The CAL-developed pressure transducers used in this test employ piezoelectric crystals and are .30" x .50" diameter in size. They have a wide range of operation (linear from .1 psi to 20 psi or higher) and are relatively insensitive to acceleration affects (.003 psi/g) due to a dual element acceleration compensation feature. In addition, to further minimize acceleration effects, the transducers were mounted on heavy seismic masses attached to the model only by a soft rubber orifice tube and light wire spring. Thermal shielding of the transducer components (particularly on the interstage) minimizes temperature effects during the short duration of the test. The output of each transducer is fed to a high impedance cathode follower whose output is amplified, displayed on an oscilloscope, and photographed.

Nozzle supply pressure (combustion pressure) was measured by means of a Kistler piezoelectric transducer and similarly displayed and photographed.

Heat transfer rates were determined by a technique that relies on sensing the transient surface temperature of the model.[3] The sensing element is a thin ($\sim$ 0.1 micron) platinum strip fused on a pyrex substrate which conforms to the local surface of the model. Since the heat capacity of the gage is negligible, the film temperature is equal to the instantaneous surface temperature of the pyrex substrate, related to the heat transfer rate to the model by the theory discussed in References 3 and 9. Typical operating environments are also given in Reference 9. The output of the heat transfer gage is fed through an analog network which converts the signal from one representing temperature to a signal directly proportional to the instantaneous heat transfer rate. This conversion is normally applicable only over the range of temperatures where the physical properties of the substrate remain constant. Outside of this range, the data must be corrected by means of procedures discussed in Section IV of this report. The signal from the analog network ($\dot{q}$ meter) is then amplified and presented on an oscilloscope and recorded photographically.

SECTION II (Cont'd) TEST EQUIPMENT

Model sketches and photographs shown in Figures 12 through 17 show location of pressure and heat transfer instrumentation on the heat shield and thrust structure, interstage walls, and blast deflector.

SECTION III TEST PROCEDURE

A. Calibration

The pressure transducers were calibrated (i.e. voltage output vs. applied pressure) after installation in the model. The voltage variation of the transducers is linear over the range of pressures normally encountered in testing. These calibrations, in conjunction with estimated values for the model pressures to be experienced during the actual test, also provide the basis for adjusting the gain of the data recording system to achieve maximum "readability" of the oscilloscope traces. At the completion of the test program the transducers were recalibrated for comparison purposes.

B. Test Program

The complete test program and test conditions are summarized in Tables I and II. Among the effects studied were vent area, shape, location, and number; longitudinal separation distance between stages; engine gimballing and one engine out; one vent panel not out; blast deflector configuration; separation plane location and over-all interstage length; heat shield shroud configuration; combustor pressure and O/F ratio; and ambient altitude. Except for the vent area, shape, and location effects, all runs were made with a standard eight triangular vent configuration.

Separate components were made to simulate the various vent configurations. Instrumentation was shifted from part to part as dictated by the test requirements. As mentioned previously, a sting support was used to support the interstage during the separation runs.

SECTION IV DATA REDUCTION

A. Pressure

The pressure transducers measure the difference between the initial ambient pressure in the chamber and the applied local pressure. The initial pressure is added to the measured pressure to obtain the absolute model pressure. To provide a common basis for comparison, all pressures are normalized by ratioing them to the combustor pressure.

B. Heat Transfer

The "thin-film" heat transfer gage is a resistance thermometer which reacts to the local surface temperature of the model. The theory of heat conduction in a homogeneous body is used to relate the surface temperature history to the rate of heat transfer[3]. Assuming that the temperature sensed by the element is the surface temperature and that a first order correction for element thickness will be adequate, the solution for the surface temperature as a function of time is:

$$T(t) = \frac{1}{\sqrt{\pi c_2 \rho_2 k_2}} \int_0^t \frac{\dot{q}(\lambda)\, d\lambda}{\sqrt{t-\lambda}} - \dot{q}(t)\, \frac{\ell}{k_1} \left(\frac{c_1 \rho_1 k_1}{c_2 \rho_2 k_2} - 1 \right)$$

where k is the thermal conductivity, c the specific heat, ρ the density, and ℓ the thickness of the film; λ is a variable of integration; and subscripts 1 and 2 refer to the metal film and the pyrex substrate, respectively.

When the above equation is properly inverted to express the heat transfer rate as a function of temperature and time, it can be programmed into a digital computer for solution. However, considerable effort is involved in converting the raw temperature-time data into a form suitable for insertion into the computer program. To overcome this restriction, an analog network has been devised[13] to convert the temperature signal directly into a heat flux rate in real time for presentation on the oscilloscope.

In view of the large quantity of data that would be gathered during this program, it was decided in the pretest planning that all heat transfer data would

SECTION IV (Cont'd.) DATA REDUCTION

be obtained directly by employing the analog networks.* Even though corrections must be applied to the data under certain conditions (as discussed below) to obtain true heat transfer rates, there is an economic and time advantage in using these networks over the more conventional digital data reduction procedure.

Two corrections of major importance must be applied to the recorded analog data to obtain a true final heat transfer rate. The first of these takes into account run-to-run changes in gage sensitivity resulting from erosion of the platinum element. It should be noted here that, for normal installation of the thin film gages in surfaces parallel to the flow, significant erosion is rarely encountered. However, in this particular application, the gages installed in the blast deflector or along the interstage walls were subjected to sustained direct impingement of rocket combustion gases for comparatively long periods of time and could experience appreciable surface erosion. Fortunately, essentially all of this erosion occurred after the conclusion of the useful combustion time during the "blow-down" of the charge tubes and did not effect the data obtained during the test period.

Continuous replacement of the eroded gages with new ones after each run, although possible, was considered economically impractical. Furthermore, previous investigations at CAL had shown that suitable corrections may be included in the data reduction procedures to account for these resistance changes. Specifically, it has been shown that the temperature coefficient,

$$\alpha \left(= \frac{\% \text{ change in resistance}}{\text{unit temperature change}} \text{ or } \frac{\Delta R/R}{^\circ F}\right),$$

for any given gage remains constant even through the gage base resistance may vary considerably (as a result of erosion, for instance).

*Subsequent to the completion of the test program it was decided that some actual temperature-time histories would be desirable to allow a more comprehensive analysis of the data. Since no data of this sort had been obtained during the test program, procedures were established to convert the analog $\dot{q}$ histories back to equivalent temperature histories. The details and results of these procedures are summarized in Appendix A.

SECTION IV (Cont'd.) DATA REDUCTION

Writing the above relationships in an alternate form, we have $\alpha R = \frac{\Delta R}{\Delta T} = K =$ gage sensitivity. It follows that since α is constant, then $K_2 = K_1\left(\frac{R_2}{R_1}\right)$. This says that a given percentage change in gage resistance is reflected as a like percentage change in the gage sensitivity. Thus, if the initial gage resistance is R_1 with a gage constant K_1 and the new resistance subsequently increases to R_2, then the new gage constant K_2 may be readily found from the above expression. This correction has been found valid even in such extreme cases where $R_2/R_1 \approx 5$.

As a consequence of the above observations, it was possible to continuously correct the gage sensitivities to account for gage erosion. This was accomplished by continuously monitoring and recording gage resistances on a run-to-run basis.

A second correction necessary to the recorded analog heat transfer data which must be considered is discussed in Reference 9. Specifically, it is shown in Reference 9 that the $\dot{Q}$ analog circuits will provide correct heat transfer values only over the range of temperature for which thermal properties of the resistance element and substrate can be considered constant. Outside of this range, a correction must be made to the data to obtain the proper result. This first-order correction accounts for two factors: (1) the variation of $(\rho c K)_2$ with temperature and (2) the nonlinear resistance-temperature characteristics of the platinum film. Values for these correction factors are presented in Figure 18 as a function of time and heat rate. The curves are labeled in terms of measured $\dot{q}$ while the ordinate gives the percentage incremental correction to be added to the measured quantity. Such corrections were applied to the heat transfer data where required.

All heat transfer data were normalized to a nominal combustor pressure of 300 psia (with the exception of the "chamber pressure buildup" series where the heat transfer values were normalized to the nominal combustor pressure appropriate to the specific run) by multiplying the corrected heat transfer rate by the ratio of the nominal combustor pressure to the actual combustor pressure. Previous experience has shown this to be a valid procedure when the combustion pressure does not vary more than five percent as was the case in these tests.

SECTION V DISCUSSION OF RESULTS

A. General Comments

1. Pressure

It has been concluded in Reference 10 that a quantitative flow model for even a simple 4-engine cluster configuration is difficult to attain although a qualitative model based on the theory of Korst[11] appears feasible. Extending the flow model from a simple 4-rocket cluster operating in a vacuum to a 6-rocket cluster operating in a semi-confined environment increases the complexity to the point where it is exceedingly difficult to visualize even a qualitative flow model. For example, as the stage separation distance increases or vent areas change, it is difficult to predict the nature of changes in the flow pattern and further what the resultant effect should be at a specific instrumentation location. Thus, even for a general area of the model such as the interstage wall, individual locations may in some cases indicate variations quite different from other locations. On the basis of these considerations, it should be recognized during any analysis of the data presented herein that such differences may well exist and that different trends at individual instrument locations should not arbitrarily be attributed to measurement errors or experimental inaccuracies.

In general, the quality of the pressure data appear excellent as can be observed from the typical oscilloscope records shown in Figure 2. It may be noted that a well-defined steady pressure level was reached during the test interval. This was not universally true, however, particularly in the model regions forward of the heat shield. Because of the large cavity volume to be filled in this region, and the limited flow area between the heat shield and interstage, pressures on the thrust structure and forward side of the heat shield often did not attain a steady level during the test period. Furthermore, in spite of the generally excellent qualitative appearance of the data obtained during the program, some difficulties were encountered in making good quantitative pressure measurements. Namely, as a direct result of the severe environment to which the pressure transducers

were exposed, some of the units indicated a change in output sensitivity between the pretest and post-test calibrations. Since periodic calibrations were not made during the course of the program, the exact histories of these sensitivity changes are not known. However, previous experience has shown that an abrupt, significant change in transducer output is 1) relatively rare and 2) usually quite apparent from an examination of previous data and easily recognizable. This observation, of course, normally applies only to a consistent sequence of test runs in which one parameter is being varied in a systematic fashion and recognizable trends in the pressure level at any given location are reasonably well established. Alternately, in cases where geometry or test conditions vary sufficiently between test sequences to produce large (and often times unpredictable) variations in the pressure level at a given location, it becomes extremely difficult to recognize calibration changes or to relate them to a specific period in time if they should occur.

As a consequence of the above considerations, it is believed reasonable to assume that for those cases where transducer sensitivities did change between the start and conclusion of the test program, the sensitivities can be considered to have remained essentially constant during any given parameter variation since no apparent large inconsistencies in the data were observed. Furthermore, since past experience has shown the majority of transducer output changes to occur gradually over a period of many runs rather than abruptly (excepting, of course, those cases where the unit has been subjected to over-pressure conditions), a linear variation in transducer sensitivity with number of runs should provide a reasonable estimate of transducer output at any given time in the test program.

2. Heat Transfer

The general quality of heat transfer data is also excellent, as shown in Figure 2. As with the pressure data, levels appear to be well established by the end of the test interval. As discussed earlier, known

SECTION V (Cont'd.) DISCUSSION OF RESULTS

corrections can be applied to the $\dot{q}$-network data to account for temperature induced nonlinearities. Furthermore, since the heat transfer gage sensitivities are dependent only on the gage resistance (an easily measured quantity), gage sensitivities are accurately known for each run and are not subject to the uncertainties encountered with the pressure transducers.

As in the case with the pressure data, difficulties are encountered in attempting to relate the observed trends at several instrumentation positions with a number of parameter changes. Thus it appears that the heat transfer data can best be analyzed by examining the trends at individual instrumentation locations with respect to configuration changes. A tendency toward a lack of correlation between heat transfer and pressure measurements at the same location also tends to point up the unpredictable and turbulent conditions in a fire-in-the-hole configuration.

B. Pressure and Heat Flux Distribution in the Interstage Region (General)

The pressure and heat flux distribution on the interstage wall is observed to follow a trend of sharply decreasing pressure and heat flux with distance above the deflector for the first few inches (model scale) and a more constant distribution over the upper regions. The general shape of the distribution in this area is largely unaffected by configuration changes, although the absolute magnitude of the heat flux and pressure measurements are affected considerably. Interstage wall pressures near the blast deflector are usually 5 psia or less, but occasionally reach nearly 8 psia. Corresponding heat fluxes are usually less than 300 BTU/ft^2-sec with an occasional maximum of almost 550 BTU/ft^2-sec. Interstage pressures are always sufficiently high to cause choked flow in the vents.

Generally speaking, the stagnation conditions upstream of the blast deflector tend to produce similar qualitative trends on the blast deflector somewhat independent of configuration. Heat fluxes and pressures tend to show maximums at about 1/3 the deflector radius, with values as high as

SECTION V (Cont'd.) DISCUSSION OF RESULTS

700 BTU/ft^2-sec and 8 psia for the heat transfer rates and pressure levels, respectively.

Heat shield pressure and heat flux distributions show consistent trends with the highest values occurring at the center and diminishing toward the edge. Maximums of measured pressure are usually less than 6 psia, 4 psia and 3 psia for the heat shield center, edge and back side respectively. Heat fluxes measured are usually less than 300 BTU/ft^2-sec and 100 BTU/ft^2-sec at the center and edge of the heat shield, respectively.

Thrust structure pressure measurements are of doubtful validity due to difficulties mentioned previously. Heat flux rates to the thrust structure are usually equal to or less than these measured on adjacent portions of the interstage wall and seldom exceed 50 BTU/ft^2-sec.

Vent rake impact pressure usually showed a consistent trend of uniformly decreasing pressure with distance above the bottom of the vent and only rarely exceeded 4 psia.

C. Vent Configuration Effects

1. Vent Area

The general effect of increasing vent area is to reduce interstage wall pressures and heat fluxes as shown in Figures 19 through 21, which present pressure and heat transfer distributions on the interstage wall as a function of vent area. Figure 22 is essentially a cross plot of Figure 19, showing the manner in which the pressure at distinct locations on the interstage wall vary with vent area. Some interesting observations can be made from an examination of this figure. For instance it can be seen that the pressures at locations $P_1 \rightarrow P_4$ (all normally above the vent openings except for the largest vent area cases) decrease in direct proportion to the increasing vent area. Alternately, the pressure in the vent leg region (particularly P_6 which is close to the blast deflector)

SECTION V (Cont'd.) DISCUSSION OF RESULTS

tends to remain constant with the smaller vent areas and then decrease in the same manner as the other pressures for larger vent areas.

Also shown in Figure 21 is an estimated variation of the average vent total pressure with vent area based on flow continuity considerations; that is,

$$\rho_N A_N u_N = \bar{\rho}_V A_V u_V \qquad \text{or} \qquad \frac{p_R A_N M_N}{\sqrt{T_R}} = \frac{\overline{p_{t_V}} A_V M_V}{\sqrt{T_{t_V}}}$$

Since the nozzle throats and vents have sonic flow ($M_N = M_V = 1$), and $T_R = T_{t_V}$, then

$$\frac{\overline{p_{t_V}}}{p_R} = \left(\frac{A_V}{A_N}\right)^{-1}.$$

As pointed out previously, all interstage wall pressures (with the exception of P_6) exhibit an identical variation with vent area, although their absolute magnitudes are smaller. It is interesting to note that P_6 (located near the vent leg/blast deflector junction) exhibits a rather strange behavior. For small vent areas, where it would be expected that P_6 would feed essentially stagnation pressure, the actual measured pressure was considerably less than the predicted value. Alternately, as vent area increased, P_6 remained constant and did not show the decreasing trend exhibited at other locations except for the largest vent areas. Furthermore, P_6 becomes considerably higher than the estimated average pressure required to pass the engine mass flow through the vents. This is consistent with pitot pressure surveys made vertically across the vent openings for other model configurations where it was found that pitot pressures near the blast deflector are considerably higher than the average value across the vent opening.

It is further interesting to note that P_6 begins decreasing proportionately with vent area at about the time the top of the vent opening

SECTION V (Cont'd.) DISCUSSION OF RESULTS

uncovers the engine exhaust planes (see Fig. 5C). Apparently at this point, a portion of the exhaust gases are free to expand and flow directly out of the vent opening without first contacting and flowing along the interstage wall, thus probably significantly altering the entire character of the interstage flow field. As was pointed out earlier, it is exactly this sort of change which makes interpretation of the experimental data so difficult. Namely, variations in vent area are accompanied by changes in the relative nozzle exit/vent opening geometry and hence attendent unpredictable changes in the interstage internal flow field.

One final observation relative to the measured interstage pressures and nozzle operating characteristics of the RL-10A3 engine should be considered. Shown in Figure 22 is the approximate (one-dimensional) exit plane pressure ratio for the RL-10A3 rocket engine; i.e., $\frac{p_{exit}}{p_c} \approx 2 \times 10^{-3}$. It may be noted that this pressure is a factor of 5 lower than the measured interstage pressure in the region of the nozzle exit (P_4) for the minimum vent area condition. It is pointed out in Reference 12 that flow through a rocket engine nozzle can be over-expanded to an exit pressure as low as 40% of ambient (i.e. $\frac{p_{exit}}{p_{amb}} \gtrapprox 0.4$) but any further expansion will result in separation of the flow from the nozzle walls. For the particular test conditions encountered here, this implies the S-IV rocket nozzles can be expected to flow full with interstage pressure ratios as high as 5×10^{-3} but probably not much higher. It follows then that for the 0.5 and possibly 1.0 sq. foot vent area cases (which includes the standard vent area also) the rocket exhaust flows were probably separated from the nozzle walls. This condition would of course change with the larger vent areas and attendent lower interstage pressures. Such operating conditions would certainly lead to completely unpredictable changes in the flow patterns in the interstage region, once again emphasizing the difficulties involved in generating even a simple interstage flow model in the presence of the many interrelated parameter variations accompanying every geometric change.

SECTION V (Cont'd.) DISCUSSION OF RESULTS

The effect of vent area changes on heat shield pressures is shown in Figure 23. It may be noted that the heat shield pressures are generally higher than the interstage wall pressure in the same region (P_4), possibly indicating the presence of considerably more reverse flow into the S-IV base region than into the forward regions of the interstage. It can also be observed that the proportionate decrease in pressure with vent area exhibited at the interstage wall is not encountered on the heat shield. In fact, vent area increases beyond 1.5 sq. feet show virtually no effect on the outer portions of the heat shield, although they do generally result in significantly lower pressures at the center of the heat shield.

2. Vent Shape

In contrast to the vent area effect is the vent shape effect wherein total vent area is maintained constant while the proportions of the rectangular vents are varied. This variation showed no significant trends. Neither is a significant trend noted as the vent location is changed as given in Table II. Although the separation of relative geometry effects from the effects due to decreasing the number of vents from 8 to 6 (same total vent area) is not possible, a trend toward higher pressures and heat fluxes is noted for the 6-vent configuration. In the eight vent configuration, only two engines are directly adjacent to a web while the remaining four engines are at least partially adjacent to a vent. For the six vent case, however, all engines are immediately adjacent to a web. This could result in a more severe blockage of the flow out of the interstage with attendent higher pressures and heating on the interstage wall.

D. Interstage and Separation Configuration Effects

Separation distance effects vary with instrumentation locations. At points high on the interstage (forward section) increasing separation distance produces a sharp decrease in pressure to very low values (see Figures 24-26).

SECTION V (Cont'd.) DISCUSSION OF RESULTS

A change in the flow pattern is suggested when the heat shield and engines begin to emerge from the interstage ($\delta_4 \rightarrow \delta_5$ separation distance) as evidenced by the rise in pressure and heat fluxes recorded on the interstage wall near the intersection with the blast deflector. This probable change in flow pattern produces no significant increase in heat flux or pressure on the blast deflector or heat shield however (see Figs. 27-28).

A sharp decrease in pressure and heat flux is initially experienced on the blast deflector with small amounts of separation, followed by comparatively constant values during the balance of the separation sequence (Fig. 27). Pressure and heat flux near the vent opening (P_{23} & Q_{43} in Fig. 27) are lowest for small separation distances and increases slightly as conditions tend to equalize across the deflector at large separation distances.

The heat shield pressures and heat flux generally show uniformly decreasing trends with increasing separation distances (see Fig. 28).

The general effect of varying the separation plane location is to produce lower pressures and heat fluxes than are encountered with the standard separation plane of 18.437 inches above the flat plate blast deflector (see Fig. 10).

Besides producing a change in the internal volume of the interstage, variations in interstage length produce corresponding changes in the distance from the nozzle exits to the blast deflector. As might be expected, the shorter interstage lengths generally give higher values of pressure and heat flux. This is especially apparent in the region of the blast deflector beneath the edge of the engine nozzles, the portion of the interstage skirt near the blast deflector, and the center of the heat shield.

E. Engine Combustion Pressure, Mixture Ratio and Ambient Altitude Effects

The effects of rocket chamber pressure shows a generally consistent trend of increasing pressure and heat flux on all components with increasing chamber pressure.

SECTION V (Cont'd.) DISCUSSION OF RESULTS

Unfortunately, no heat transfer data were recorded for the mixture ratio series. The available pressure data which included measurements at almost all locations show insignificant effects with no consistent trend.

Although altitude was varied from 120,000 feet to 240,000 feet, no significant effects were noted. The minor variations that were observed showed no consistent trends.

F. Shroud and Blast Deflector Configuration Effects

The shroud configurations were examined only at the widest separation distance (δ_6) and with the intermediate separation plane location (P_1). Since no data were obtained for this particular configuration without a shroud, comparison of the shroud data with no-shroud data is not possible. The results measured for the two shrouds do not indicate any significant differences between the cylindrical and conical shrouds.

The scalloped and cusp blast deflectors had the effect of increasing pressure and heat transfer rates on the interstage legs between adjacent vents. The probable favorable change in flow patterns produced by these formed deflectors also resulted in generally lower pressures and heat fluxes on the heat shield.

G. One Engine Out, One Vent Panel Not Out, and Gimballing Effects

An inoperative engine (engine out) causes reduced pressure and heat transfer rates on the blast deflector in the vicinity of that engine although no significant changes occurred in the upper interstage and heat shield measurements.

Gimballing the engines was found to produce relatively insignificant effects with no consistent trend to the variations that were noted.

One vent panel not out also produced insignificant effects with no trend in the variations noted.

SECTION VI CONCLUSIONS

1. The feasibility of applying short duration techniques to the experimental study of the gas dynamic processes involved in the separation of booster stages in a high altitude environment has been demonstrated.

2. Flow durations sufficient for usual high altitude base heating tests are inadequate for separation studies because of the large model cavities which must be filled. However, increased test times are allowable since vacuum chamber blast wave phenomena produce negligible effects in the semi-confined environment typical of a stage separation model.

3. Most of the parameter variations studied during the test program were not independent, but produced associated changes in model geometry. As a result, isolation of the effects of specific parameter changes and interpretation of the experimental data is a difficult task.

4. The general quality of the test data appears good. Because of the comprehensive range of geometric variables investigated and the large number of test measurements made, only a minimum number of repeat runs were conducted. Where repeat data are available, agreement is good.

5. Interstage wall pressures and heat fluxes at zero separation are consistently high near the interstage/blast deflector junction, decrease sharply a short distance above the deflector (in the region of the vents) and then become comparatively uniform over the remainder of the interstage wall. This trend is largely independent of vent or interstage geometry.

SECTION VI (Cont'd.) CONCLUSIONS

6. As a result of the stagnation conditions prevailing immediately above the flat plate blast deflector, conditions on the blast deflector are comparatively unaffected by interstage geometry changes. Maximum heat transfer and pressures occur at approximately one-third of the deflector radius, or considerably inboard of the projected rocket engine centerlines.

SECTION VII REFERENCES

1. Goethert, B. H.: "Base Flow Characteristics of Missiles with Cluster-Rocket Exhausts", Aerospace Engineering, March 1961 (also IAS Paper 60-89), National Summer Meeting, June 28 - July 1, 1960.

2. Bird, K. D., Matthis, C. L. and Reece, J. W.: "The Application of Short-Duration Techniques for the Experimental Study of Base Heating, Part I: High Altitude Testing Technique and Experimental Results for a 4-Engine Rocket Configuration", CAL Report No. HM-1510-Y-1 (I), April 1962.

3. Vidal, R. J.: "Transient Surface Temperature Measurements", CAL Report No. 114, March 1962.

4. Martin, J. F., Duryea, G. R., and Stevenson, L. M.: "Instrumentation for Force and Pressure Measurements in a Hypersonic Tunnel", CAL Report No. 113, Presented at Second National Symposium on Hypervelocity Techniques, Denver, Colorado, Marcy 19-20, 1962.

5. Rickard, W. D. and Dennis, R. J.: "High Altitude Base Heating and Pressure Distribution Investigations on the Saturn S-IV 6-Engine Stage Rocket Using Short-Duration Techniques", CAL Report No. HM-1510-Y-3, June 1963.

6. Matthis, C. L., Muench, R. K., and Rickard, W. D.: "The Design and Development of a Short-Duration Constant Pressure Combustor for Use in Rocket Base-Heating Investigations", CAL Report No. HM-1510-Y-2, December 1962.

7. Tobias, J. A., Knapp, T. W., Barker, H. H. Jr., and Bell, D. E.: "Saturn S-I/S-IV Stage Separation Program Shock Tube Model", Douglas Report No. SM-41949, September 1962.

8. Zinsmeyer, H. G.: "Minutes of the Meeting on Pressure and Heat Transfer Tests on the S-I/S-IV Separation", MSFC Memo No. M-AERO-A-23-63, March 18, 1963.

9. Bogdan, L.: "Heat Transfer Instrumentation", CAL Report No. WTH-021, March 1963 (CAL Internal Report).

10. Carlson, D. R.: "An Analytical Study and Discussion of a Typical Four-Unit Clustered-Rocket-Nozzle Configuration at High Altitude Including Calculations for Jet Interaction at 160,000 Feet, Unpublished CAL Report, September 26, 1962.

SECTION VII (Cont'd) REFERENCES

11. Korst, H. H. and Chow, W. L.: "Compressible Non-Isoenergetic Two-Dimensional Turbulent (Pr_t = 1) Jet Mixing At Constant Pressure", U. Illinois, Eng. Exp. Sta. ME-TN-392-4, January 1959.

12. Sutton, G. P.: "Rocket Propulsion Elements", Second Edition, John Wiley & Sons, 1956.

13. Skinner, G. T.: "Analog Network to Convert Surface Temperature to Heat Flux", CAL Rept. No. CAL-100, AD 247277, February 1960; Also ARS Journal, Vol. 30, No. 6, pp. 569-570 (June 1960).

TABLE I

TEST SCHEDULE SUMMARY †

No. of* Runs	Combustion Pressure (psia)	Ambient Altitude (Ft. x 10^{-3})	Configuration**	Objective
2	300	210	A_o(Basic	Effect of Vent Area
10			$A_1 \rightarrow A_5$	
6	300	210	$A_2S_1 \rightarrow A_2S_3$	
2	300	210	A_oS_7	Effect of Vent Shape
6	300	210	$A_4S_4 \rightarrow A_4S_6$	
6	300	210	$A_2L_1 \rightarrow A_2L_1S_3$	Effect of Vent Location
4	300	210	A_2L_1, A_4L_1	
12	100	210	$\delta_1 \rightarrow \delta_6$	Effect of Chamber Pressure Build-up on Separation
12	200	210	$\delta_1 \rightarrow \delta_6$	
12	400	210	$\delta_1 \rightarrow \delta_6$	
12	300	210	$\delta_1 \rightarrow \delta_6$	Effect of Separation Distance
8	300	210	$P_1\,\delta_1 \rightarrow P_1\,\delta_4$	Effect of Separation Plane
8	300	210	$P_2\,\delta_1 \rightarrow P_2\,\delta_3, P_2\,\delta_6$	
8	300	250	$P_1\,\delta_1 \rightarrow P_1\,\delta_4$	Effect of Altitude
6	300	250	$P_2\,\delta_1$, $P_2\,\delta_2$, $P_2\,\delta_6$	
12	300	250	$\delta_1 \rightarrow \delta_6$	

TABLE I (Cont'd.)

No. of Runs*	Combustion Pressure (psia)	Ambient Altitude (Ft. x 10)	Configuration**	Objective
2	300	210	$P_1 \mathcal{O}_6 Sh_1$	Effect of Shroud
2	300	210	$P_1 \mathcal{O}_6 Sh_2$	
14	300	145	$\mathcal{O}_o \rightarrow \mathcal{O}_6$	Effect of Altitude
14	300	120	$\mathcal{O}_o \rightarrow \mathcal{O}_6$	Correlation with MSFC Data
8	300	210	$G_1 \rightarrow G_4$	Effect of Gimballing
6	300	210	$I_1 \rightarrow I_3$	Effect of Inter-stage Length
2	100	210	A_o(Basic)	
2	200	210	A_o(Basic)	Effect of Chamber Pressure Buildup
2	400	210	A_o(Basic)	
4	300	210	D_1 & D_2	Effect of Blast Deflector
4	300	210	E_1 & E_2	Effect of One Engine Out
2***	300	210	R_1 & R_2	Effect of Mixture Ratio
4	300	210	V_1 & V_2	Effect of One Vent Panel Not Out

ǂ See Table III (Volume II) for detailed test schedule.

* Two runs needed for each configuration in order to record all instrumentation.

** See Table II for explanation of configuration symbols.

*** No heat transfer data and only partial pressure data for these runs.

TABLE II

CONFIGURATION DEFINITIONS AND RANGES

Symbol	Variable	Description
A_o	Basic	8 triangular vents, total area of 1.01 ft^2 (model scale), bottom of vent even with blast deflector, interstage length of 18.437 inches (ms),* zero separation distance, flat plate blast deflector, no heat shield shroud, engines not gimballed (Nom. 6° cant), engine O/F = 5.0
A	Vent Area	Rectangular vents - same width and varying height, providing from 0.5 to 2.5 ft^2 (ms) in equal increments
S	Vent Shape	Rectangular - 1.01 and 2.0 ft^2 (ms) with three different web widths; triangular 6 vent also
L	Vent Location	Bottom of vent even with flat plate blast deflector or 1.8" above FPBD.**
δ	Separation Distance	6 distances from 1.32" to 26.80" (see Fig. 9)
P	Separation Plane	3 positions; at thrust structure, at flat plate blast deflector and 8.3 inches above FPBD
Sh	Shroud	Straight and conical (as shown in Fig. 7)
I	Interstage Length	From 17.837" to 20.837" (ms)
G	Gimballing	± pitch and ± yaw (as shown in Fig. 8)
D	Blast Deflector	Cusp and scalloped (as shown in Fig. 6)
E	One Engine Out	Engine adjacent to and between vent webs
R	Mixture Ratio	O/F = 4.0 and 6.0 (nominal ● 20%)
V	Vent Panel Not Out	Vent panel adjacent to and between engines

*ms = model scale
**FPBD = flat plate blast deflector

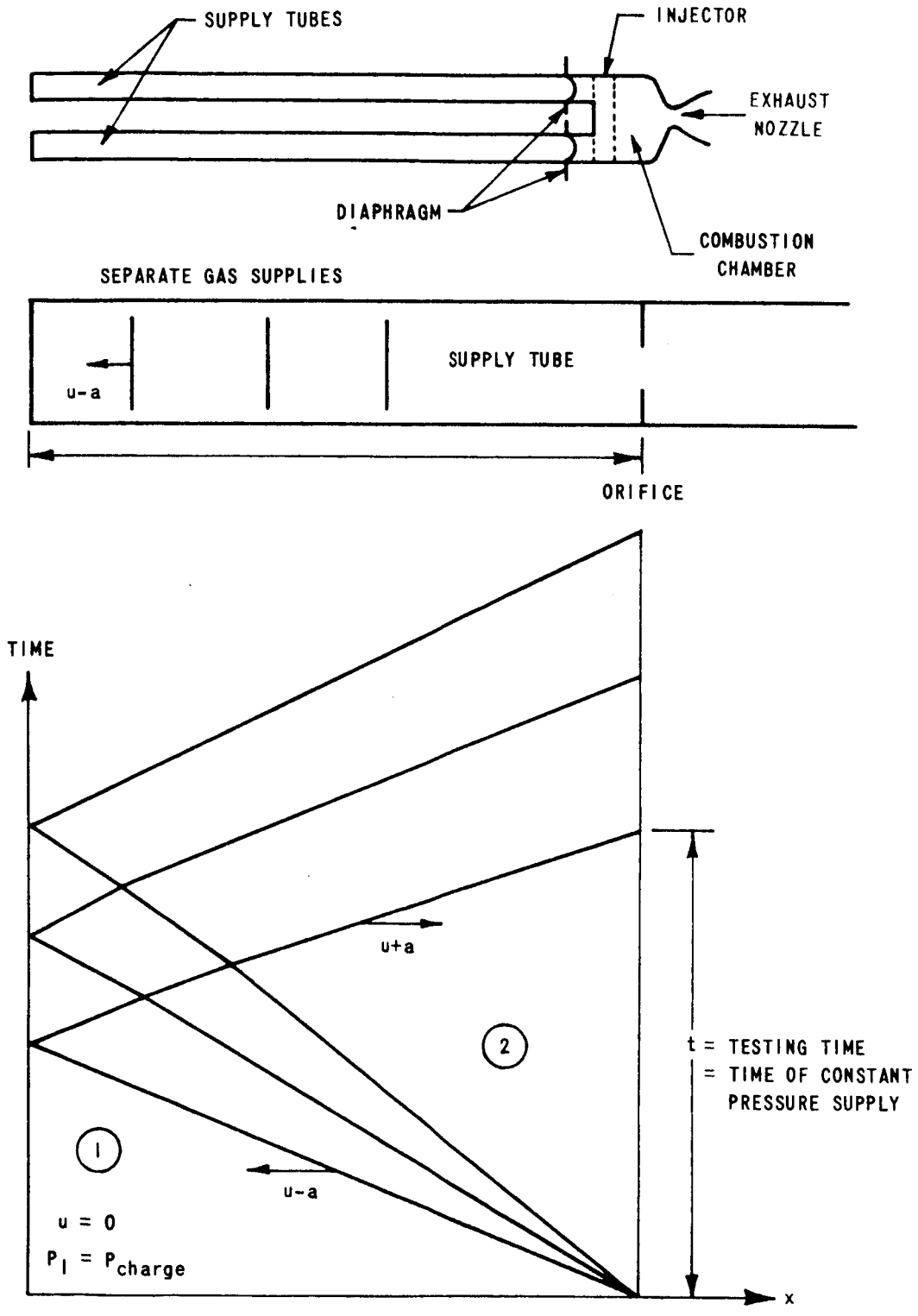

Figure I COMBUSTOR SCHEMATIC AND SUPPLY TUBE WAVE DIAGRAM

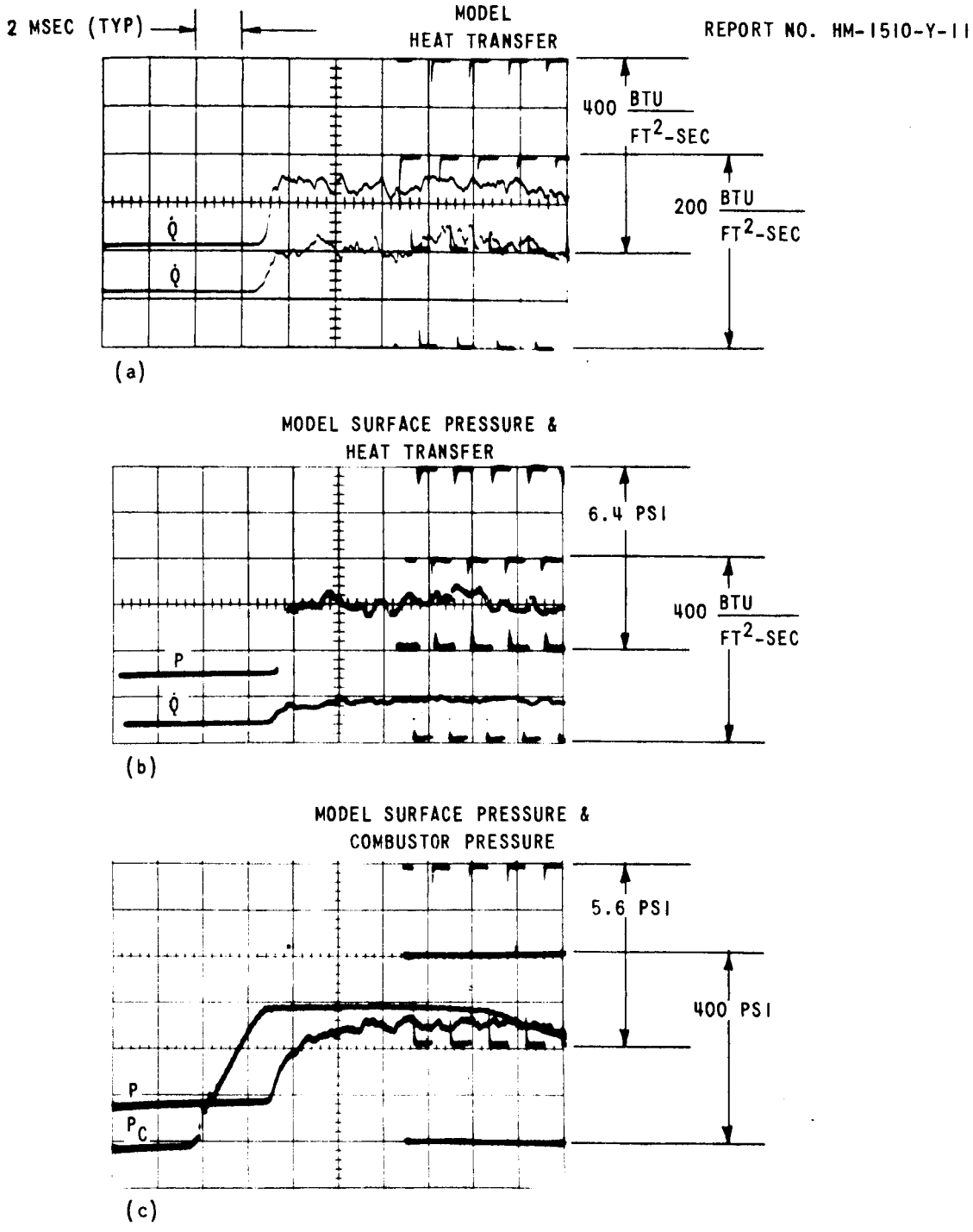

Figure 2 TYPICAL OSCILLOSCOPE DATA RECORDS
S-IV STAGE SEPARATION - HEAT TRANSFER
AND PRESSURE PROGRAM

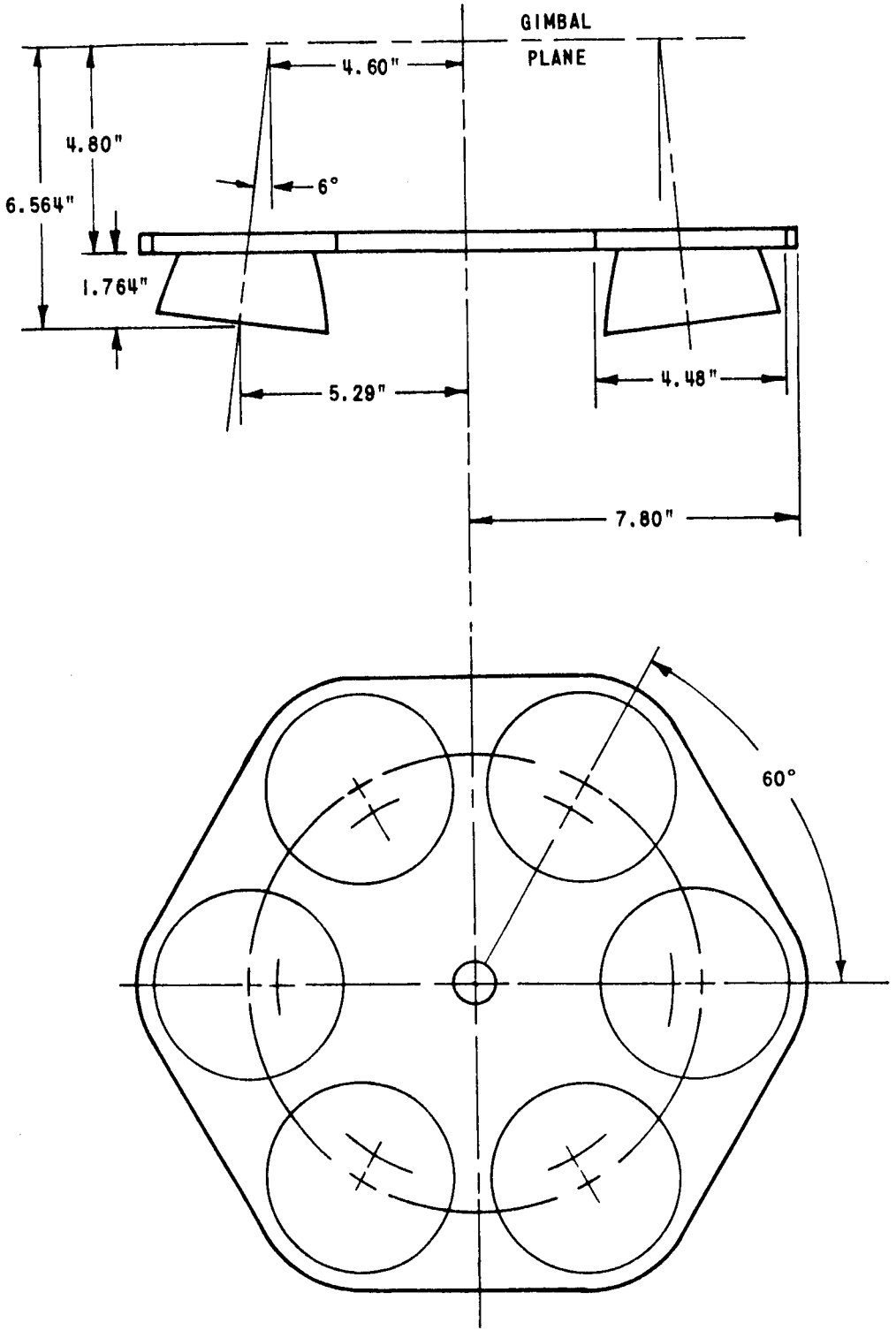

Figure 3 SIX ENGINE S-IV MODEL BASE DETAIL (FROM REFERENCE 7)

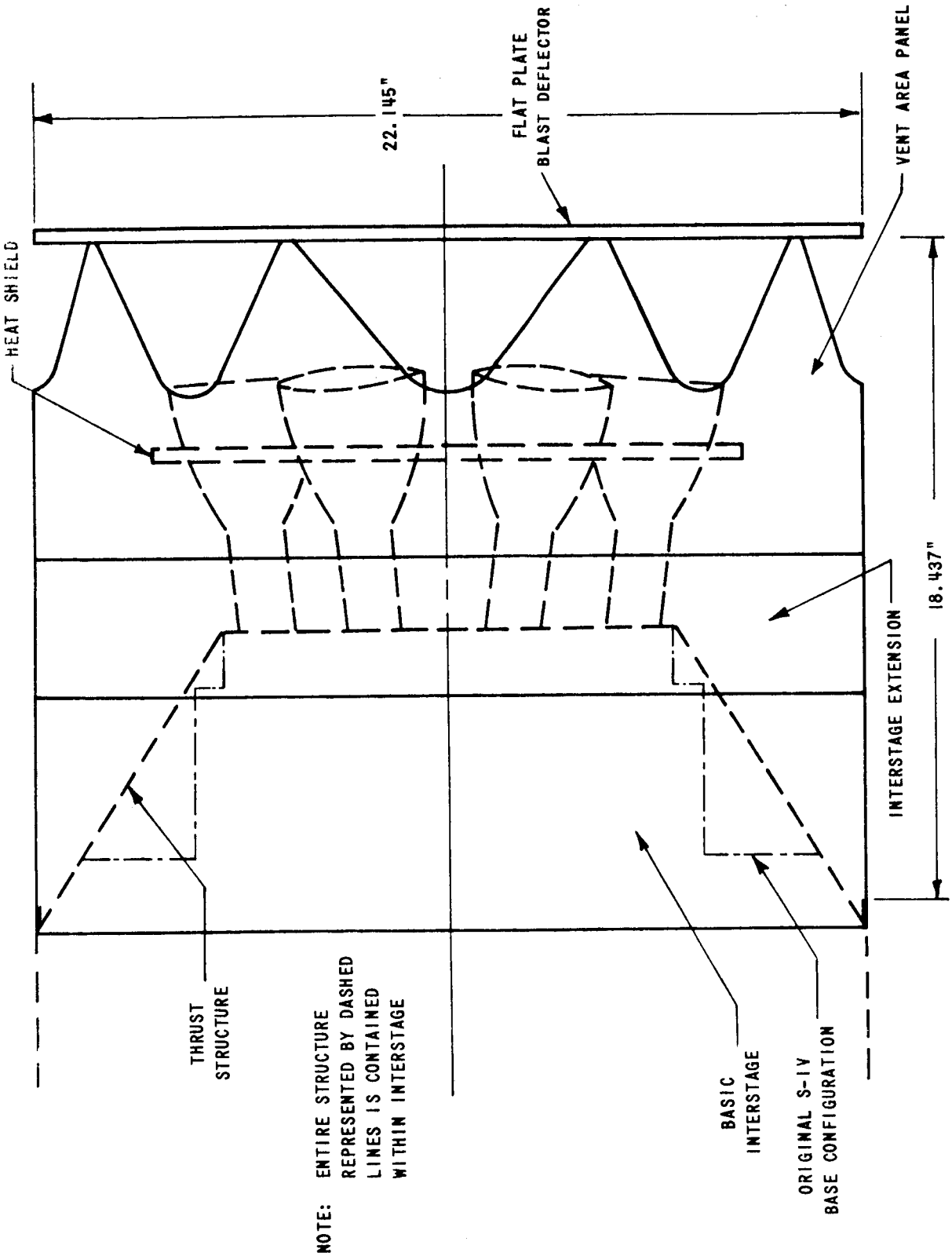

Figure 4 SEPARATION MODEL (FROM REFERENCE 7)

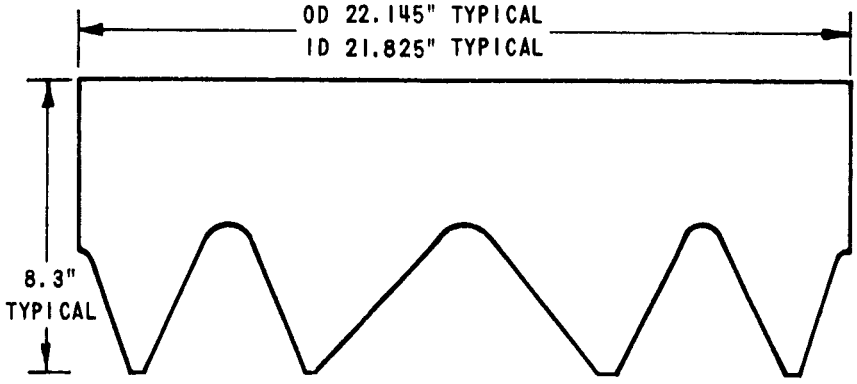

8 VENT STANDARD AREA PANEL

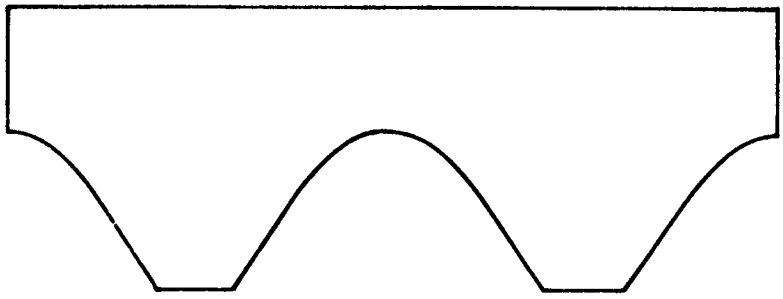

6 VENT STANDARD AREA PANEL

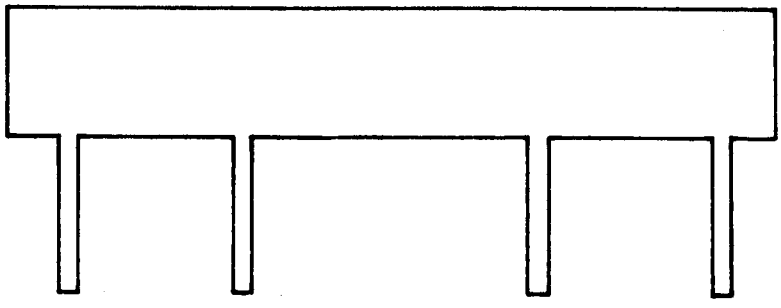

8 VENT VARIABLE AREA AND VARIABLE VENT SHAPE PANEL

NOTE: FOR DETAILS SEE FIGURE 5b

Figure 5a MODEL VENT AREA PANELS (FROM REFERENCE 7)

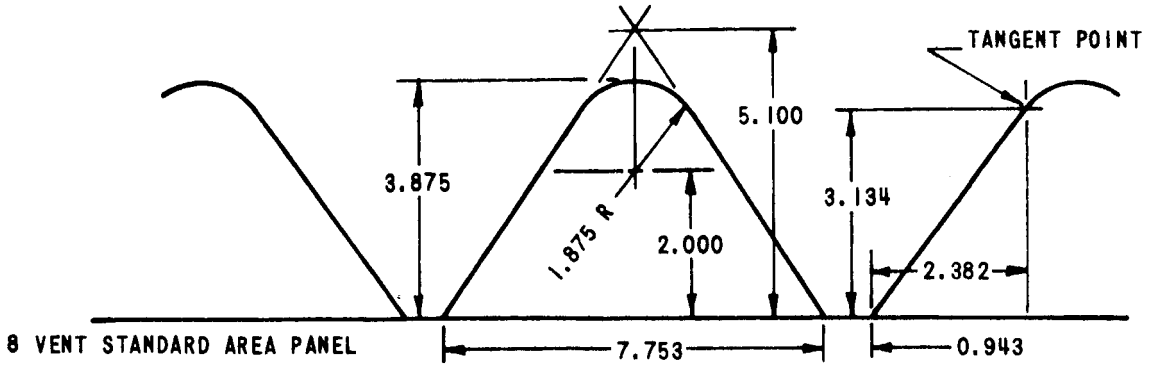

8 VENT STANDARD AREA PANEL

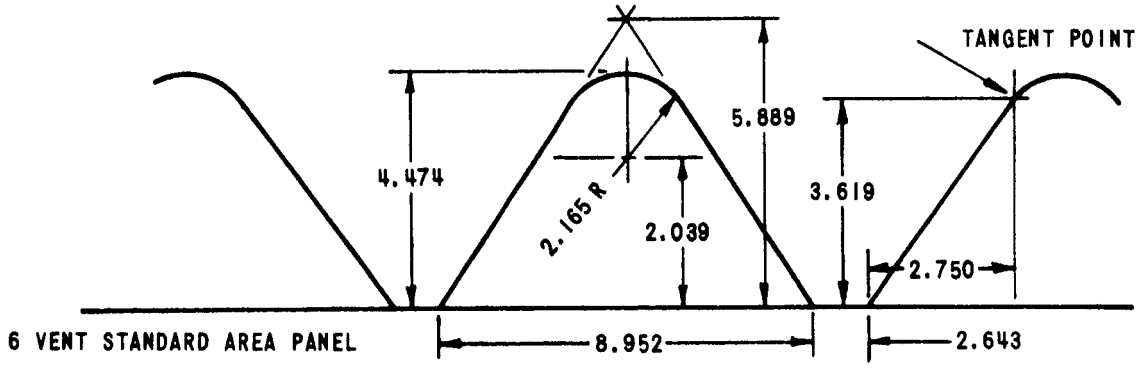

6 VENT STANDARD AREA PANEL

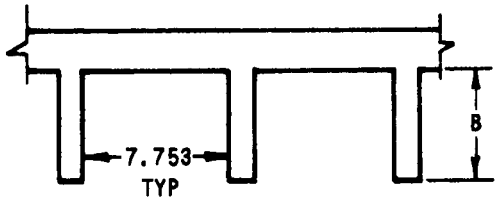

8 VENT VARIABLE AREA PANEL

VALUES OF B
1.183
2.390
3.550
4.733
5.920

DIMENSION IN INCHES

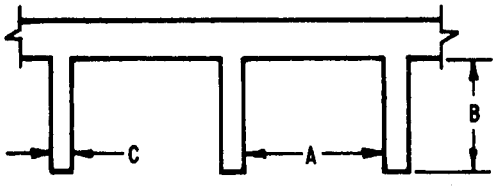

8 VENT VARIABLE SHAPE PANEL

A	B	C
6.81	2.720	1.886
6.81	5.365	1.886
5.867	3.136	2.829
5.867	6.209	2.829
4.924	3.729	3.772
4.924	7.367	3.772

Figure 5b MODEL VENT AREA PANEL DETAILS (FROM REFERENCE 8)

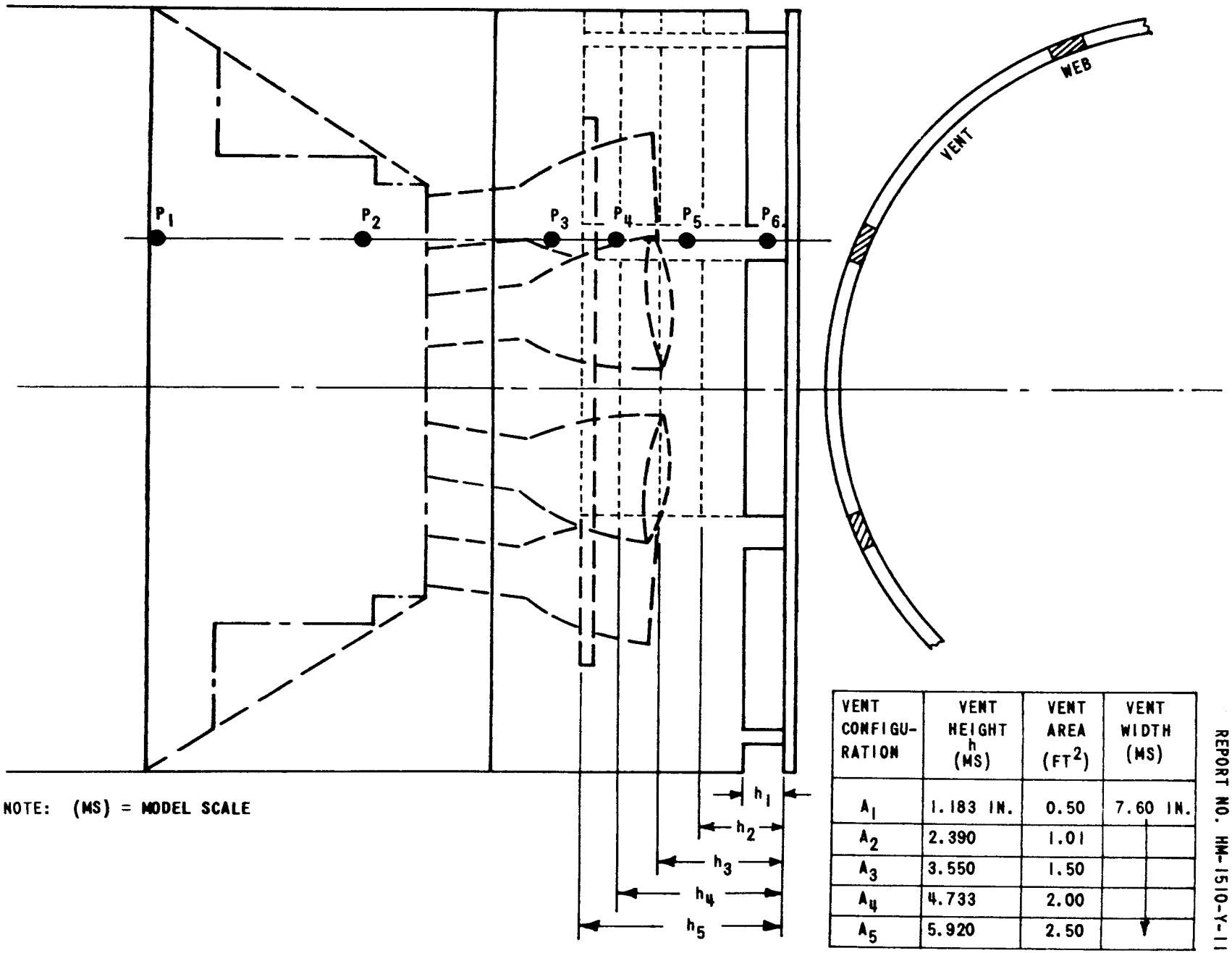

NOTE: (MS) = MODEL SCALE

VENT CONFIGURATION	VENT HEIGHT h (MS)	VENT AREA (FT^2)	VENT WIDTH (MS)
A_1	1.183 IN.	0.50	7.60 IN.
A_2	2.390	1.01	
A_3	3.550	1.50	
A_4	4.733	2.00	
A_5	5.920	2.50	

Figure 5c VARIABLE VENT AREA CONFIGURATIONS

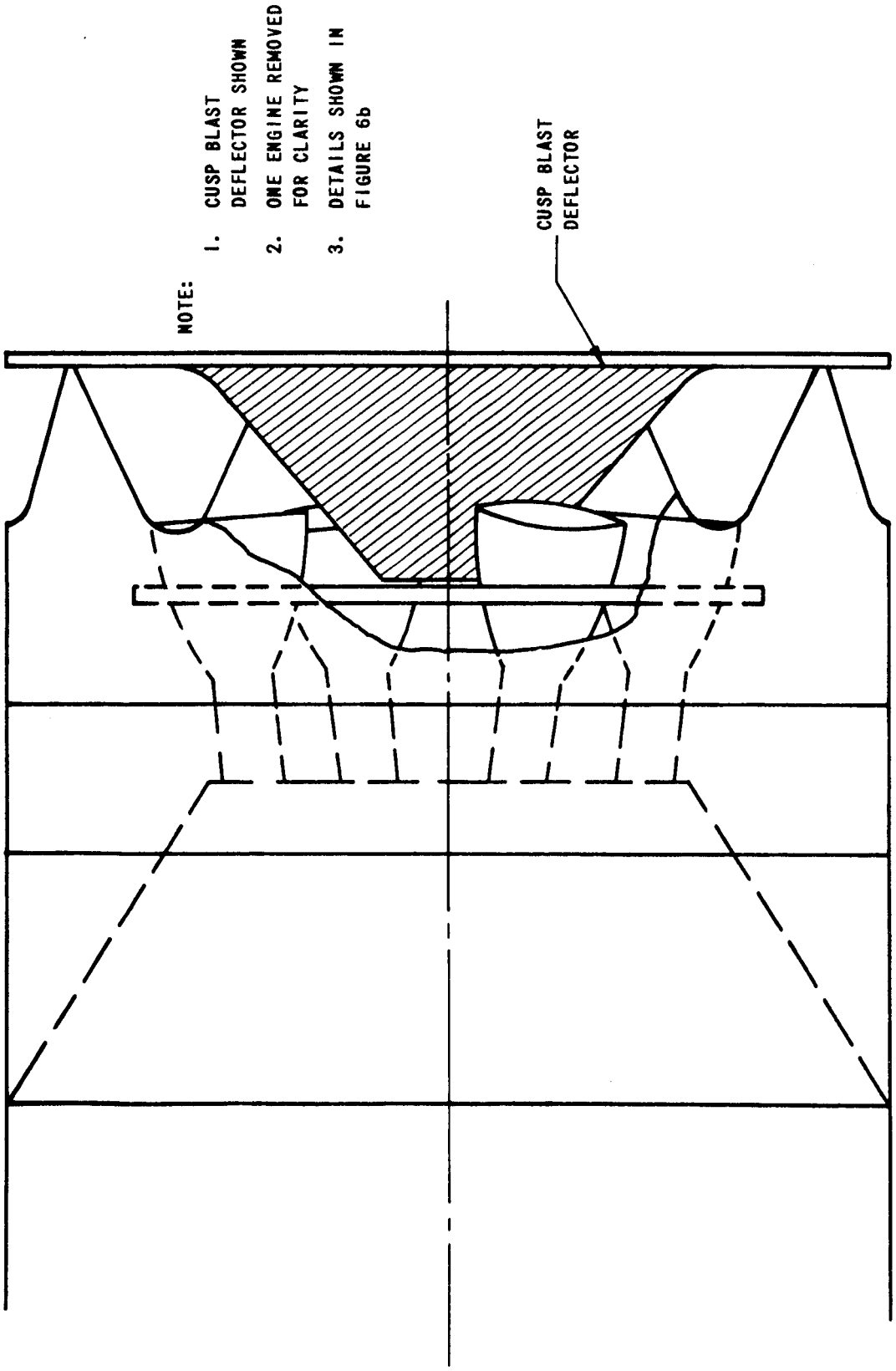

Figure 6a BLAST DEFLECTOR ASSEMBLY (FROM REFERENCE 7)

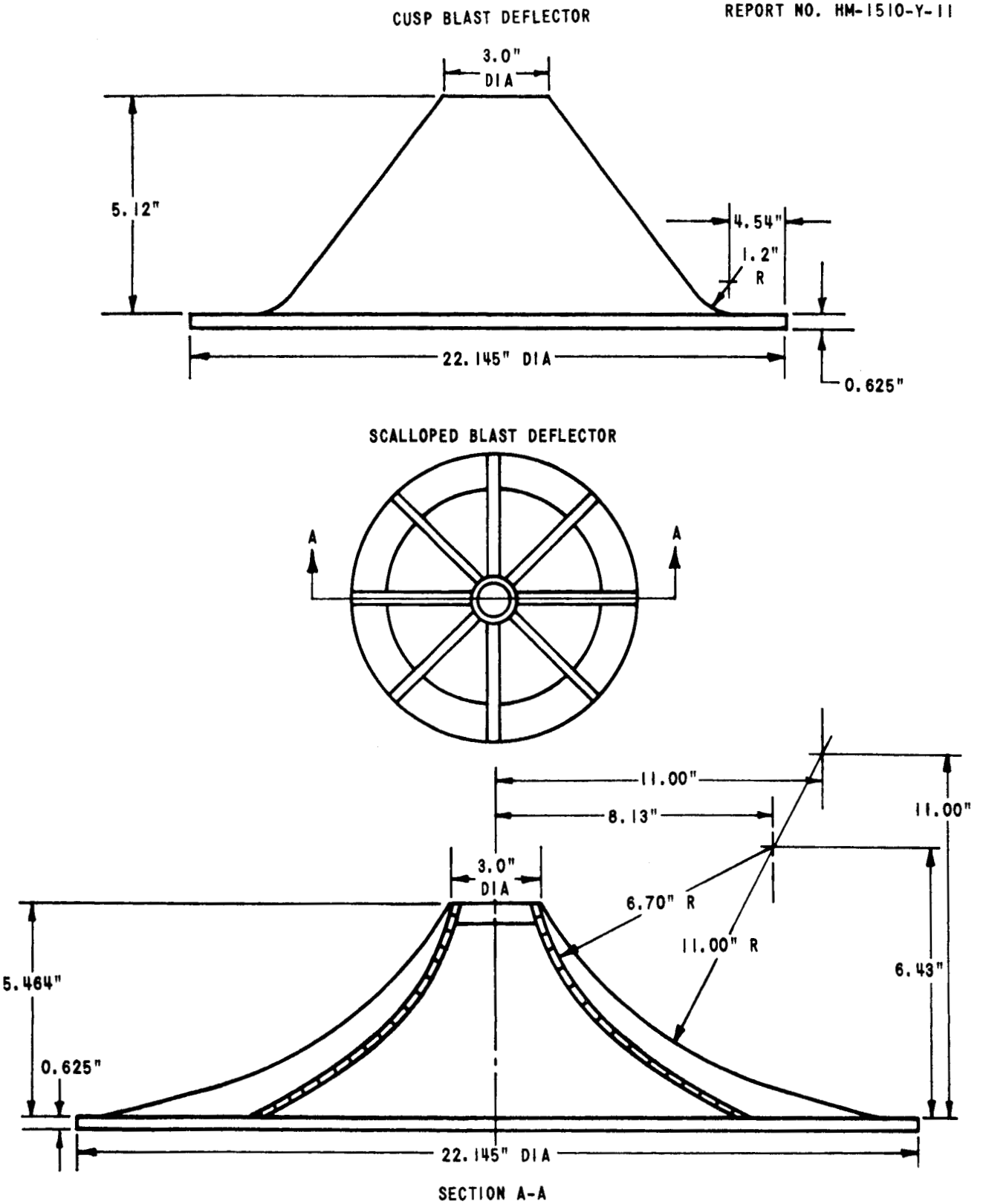

Figure 6b BLAST DEFLECTOR DETAILS (FROM REFERENCE 7)

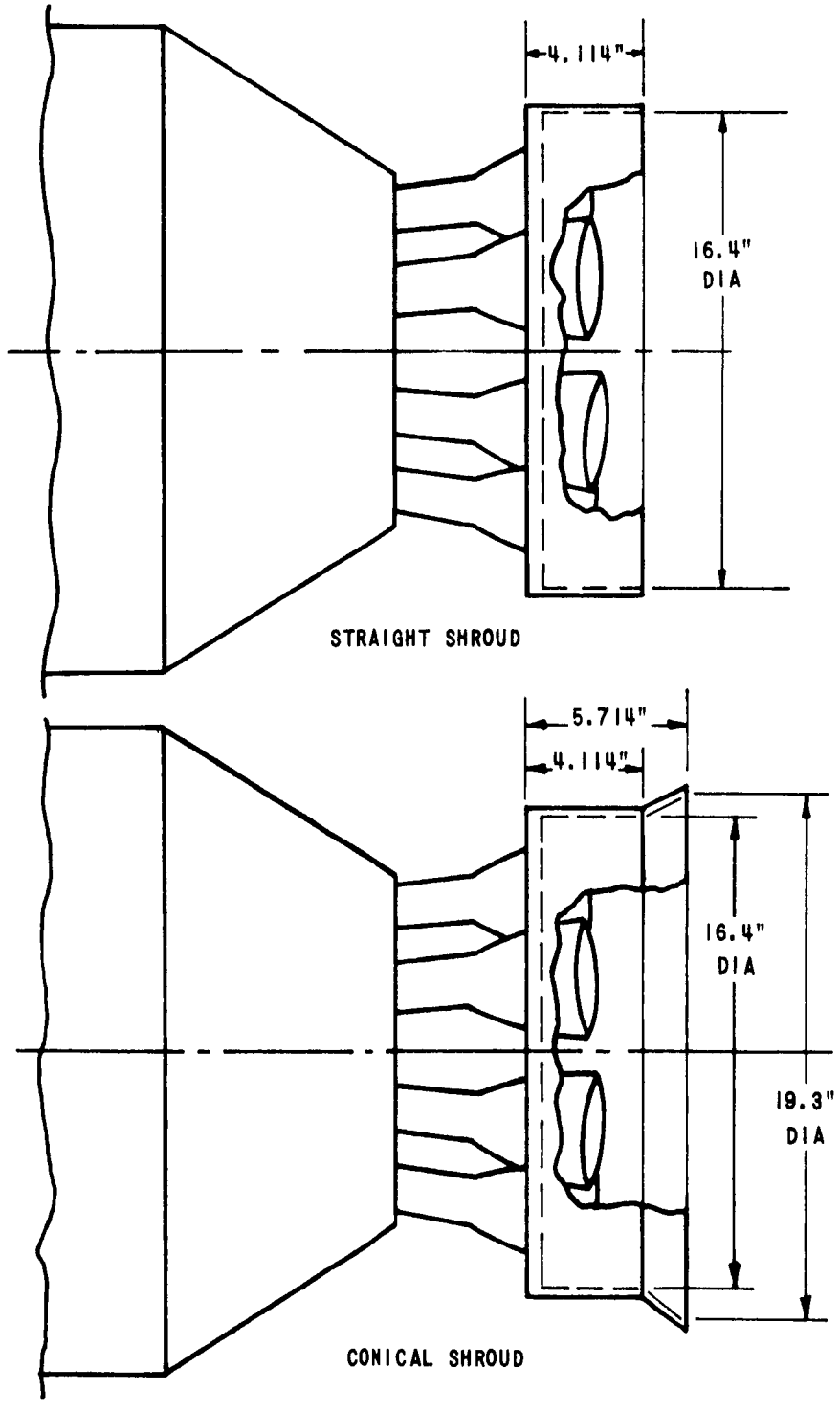

Figure 7 SHROUD ASSEMBLY AND DETAILS (FROM REFERENCE 7)

P PITCH
Y YAW
R ROLL

5.6° GIMBALLING INDICATED BY ARROW TOUCHING CIRCLE
4° GIMBALLING INDICATED BY ARROW NOT TOUCHING CIRCLE

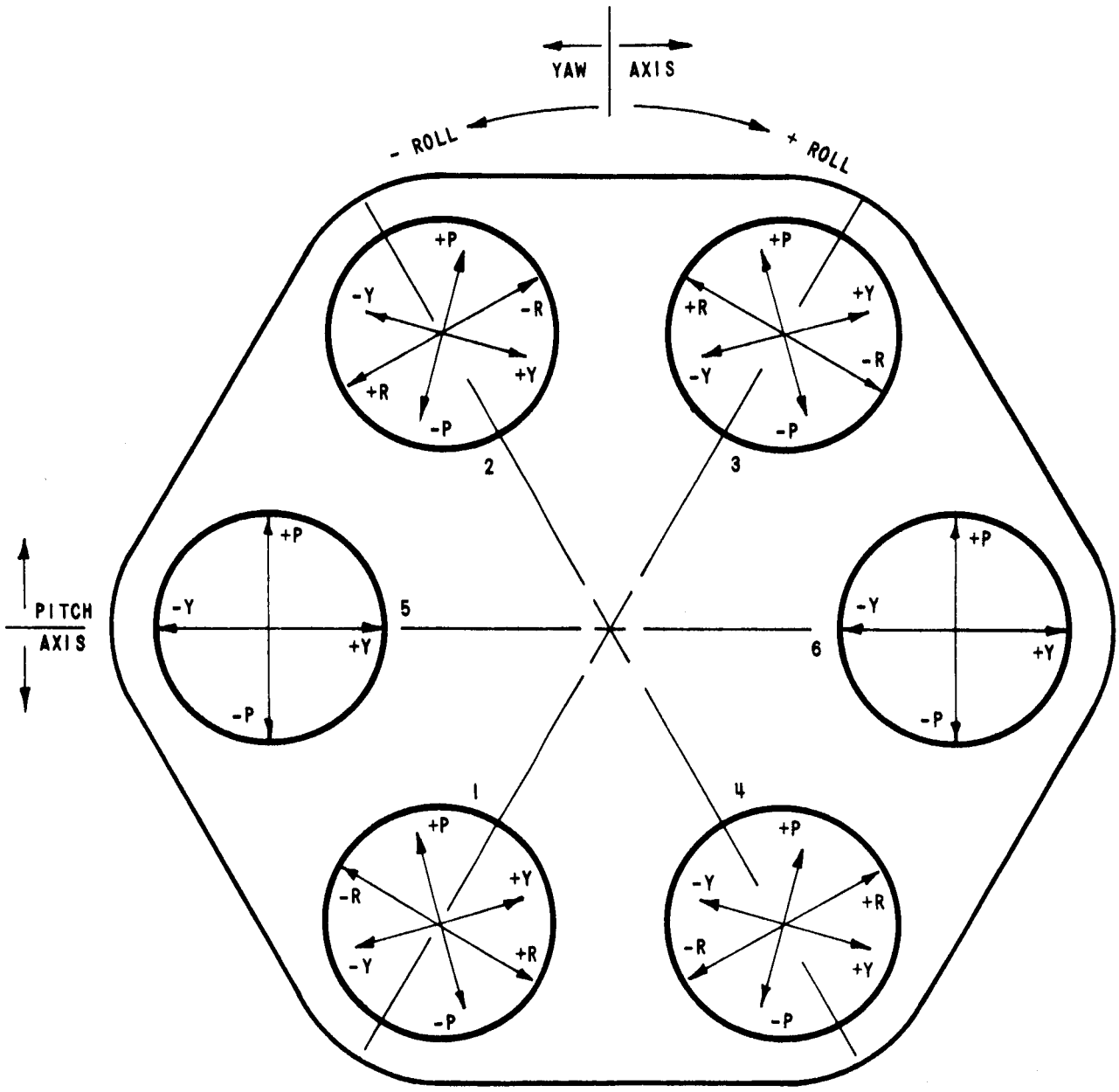

Figure 8 GIMBALLING CONFIGURATIONS

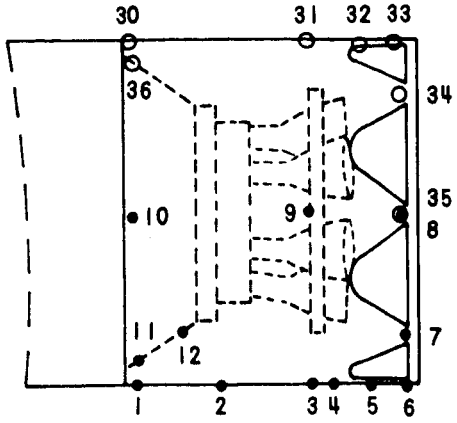

● PRESSURE TRANSDUCER
○ HEAT TRANSFER GAGE

REPORT NO. HM-1510-Y-11

SEPARATION DISTANCE

$\delta_0 = 0"$

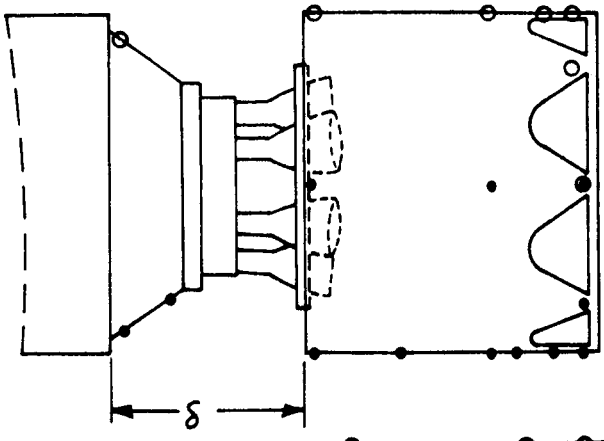

$\delta_4 = 12.7"$

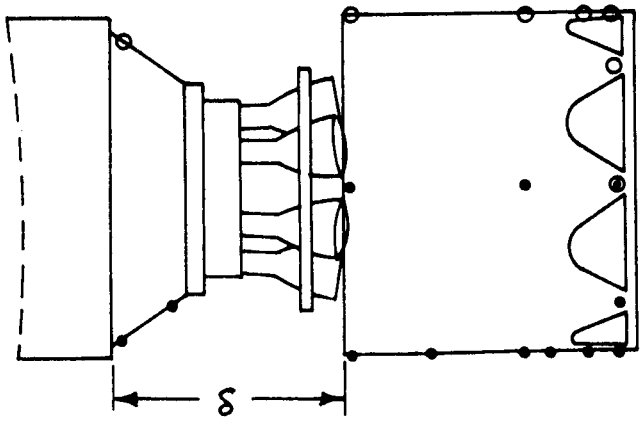

$\delta_5 = 15.0"$

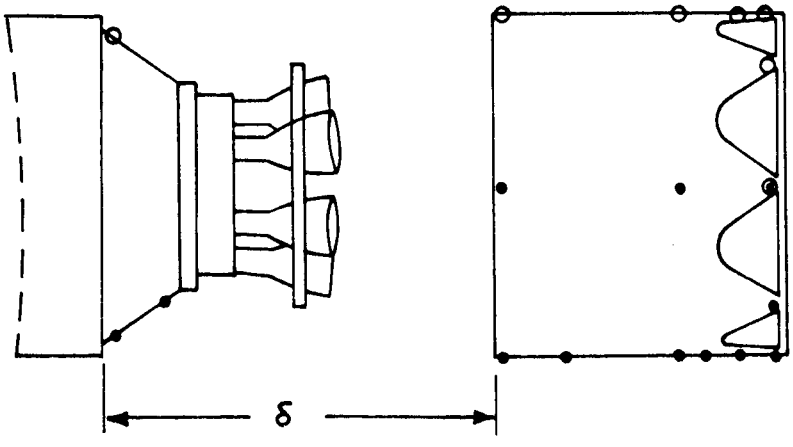

$\delta_6 = 26.8"$

Figure 9 SATURN S-I/S-IV INTERSTAGE SEPARATION

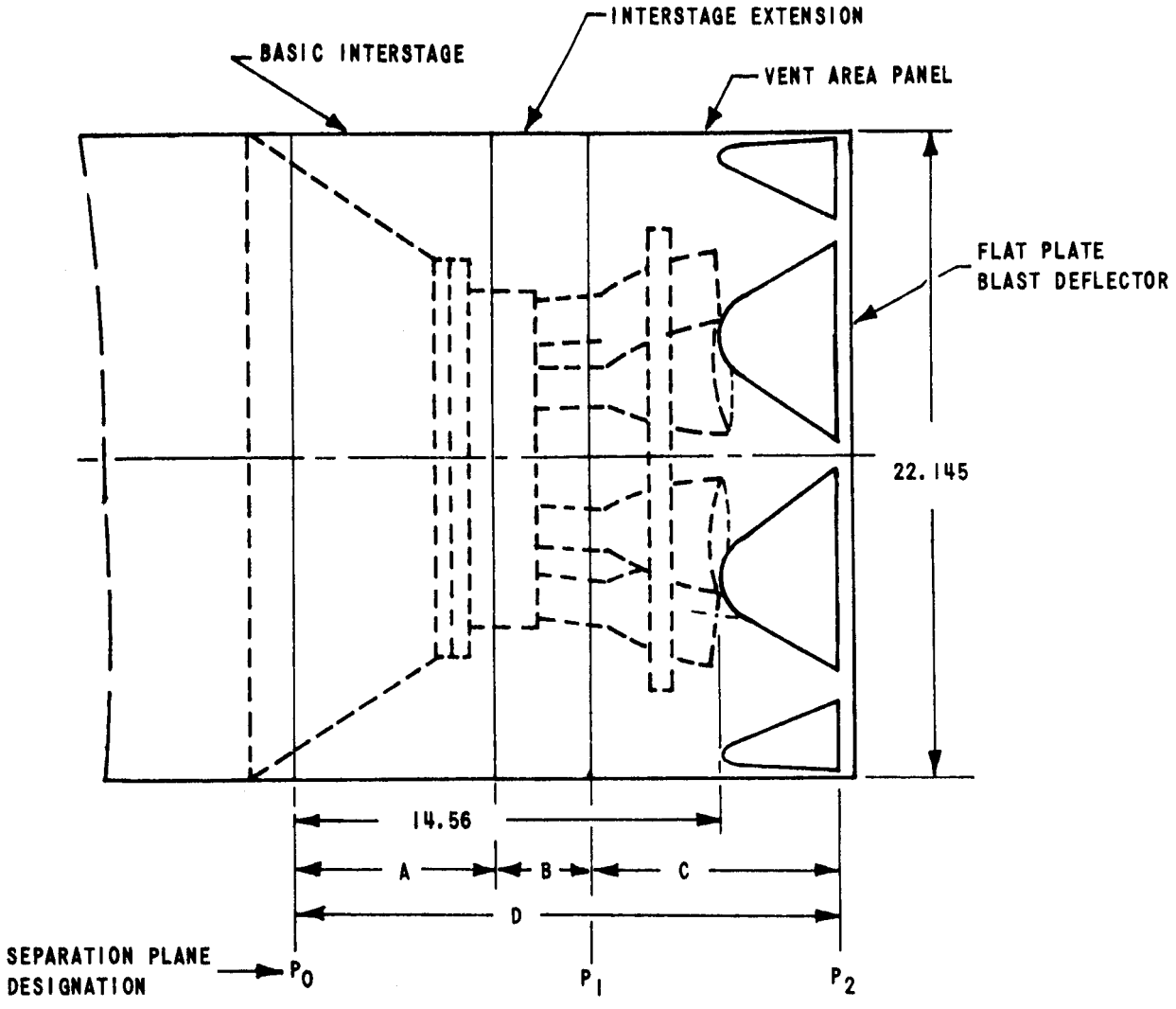

INTERSTAGE CONFIGURATION

SYMBOL	A	B	C	D
I_0	6.937	3.2	8.3	18.437
I_1	6.937	2.6	8.3	17.837
I_2	6.937	4.4	8.3	19.637
I_3	6.937	5.6	8.3	20.837

DIMENSIONS IN INCHES

Figure 10 SATURN S-I/S-IV INTERSTAGE SEPARATION PLANE CONFIGURATIONS (FROM REFERENCE 8)

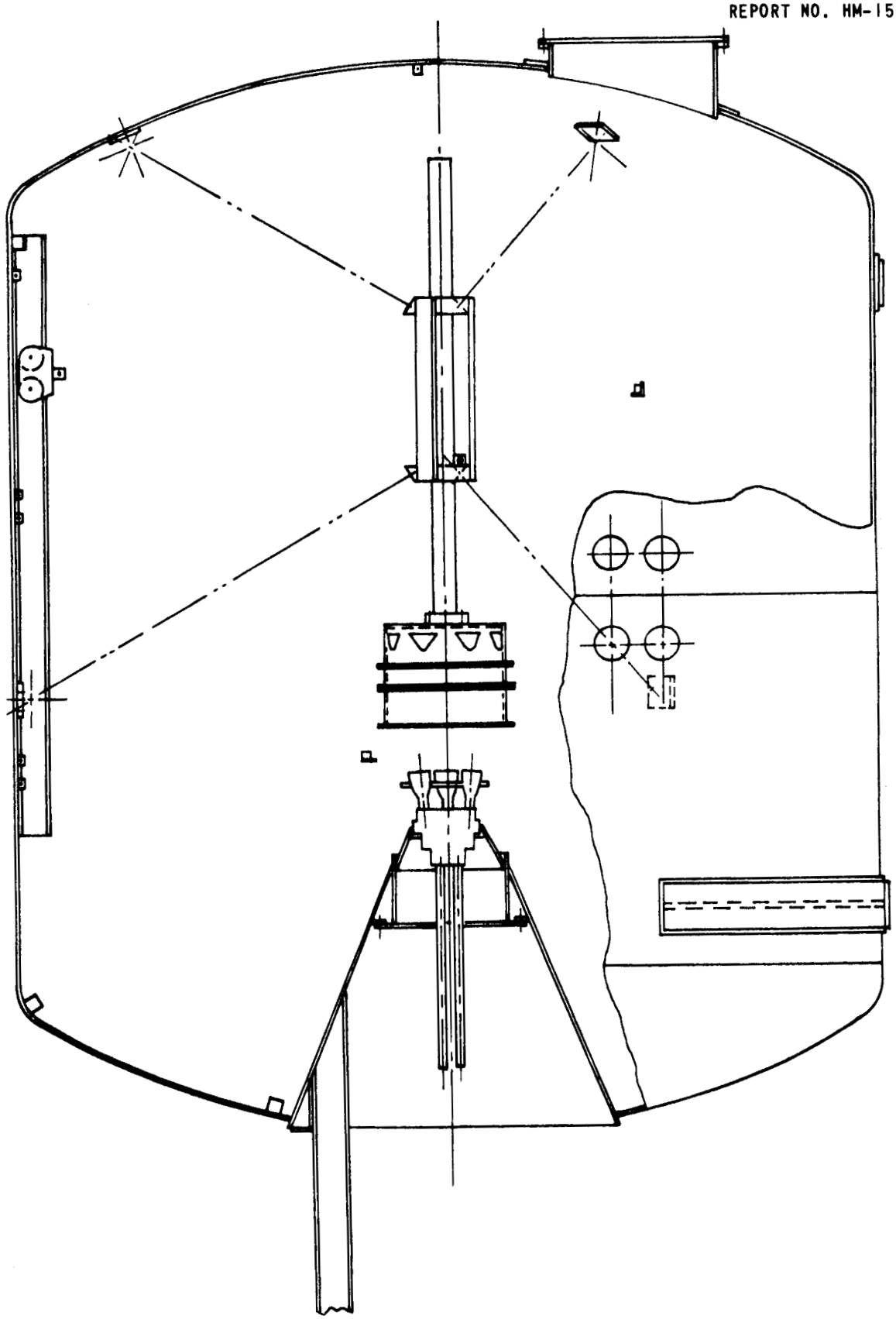

Figure 11 S-I/S-IV STAGE SEPARATION HIGH ALTITUDE TEST SETUP

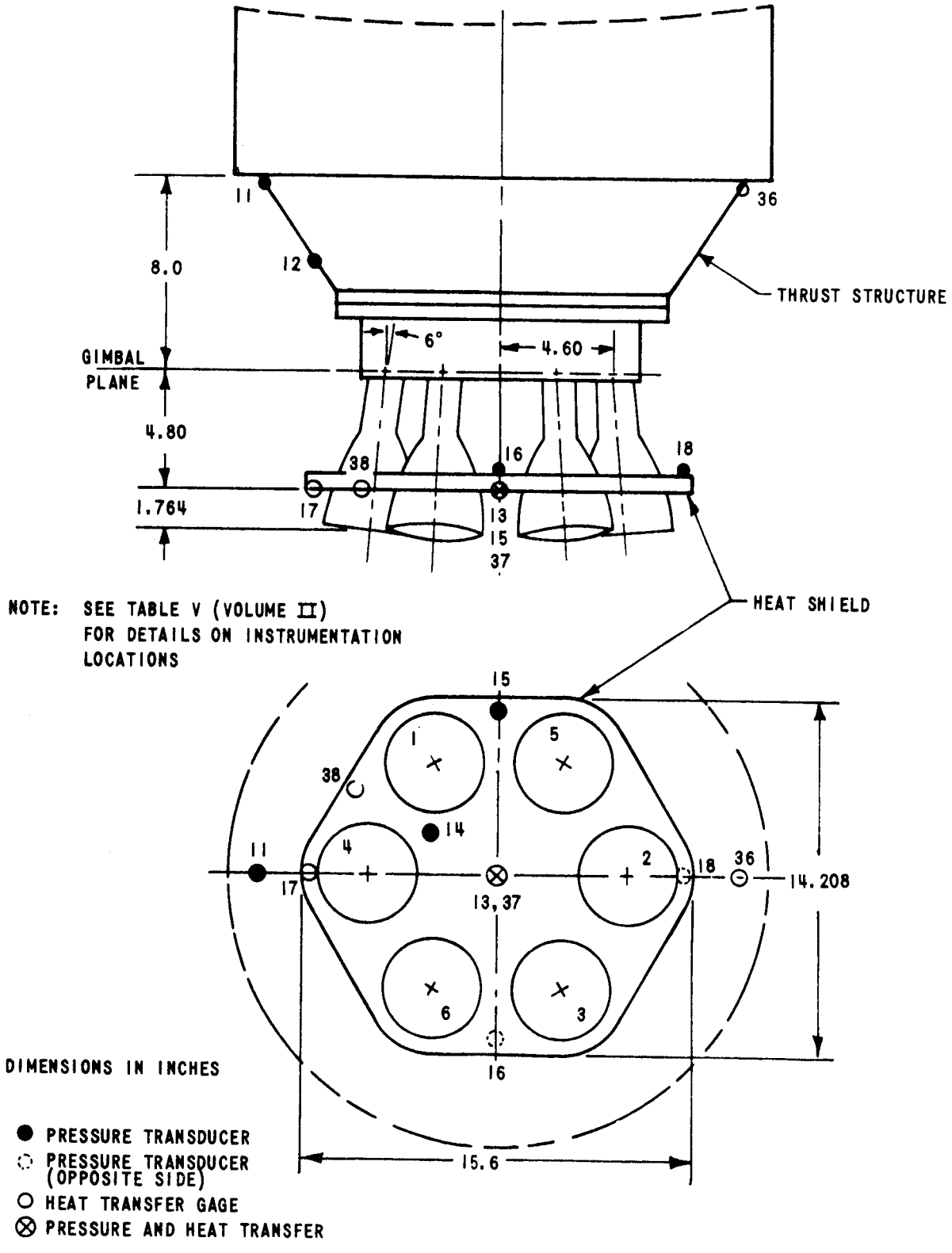

Figure 12 THRUST STRUCTURE AND HEAT SHIELD INSTRUMENTATION (FROM REFERENCE 8)

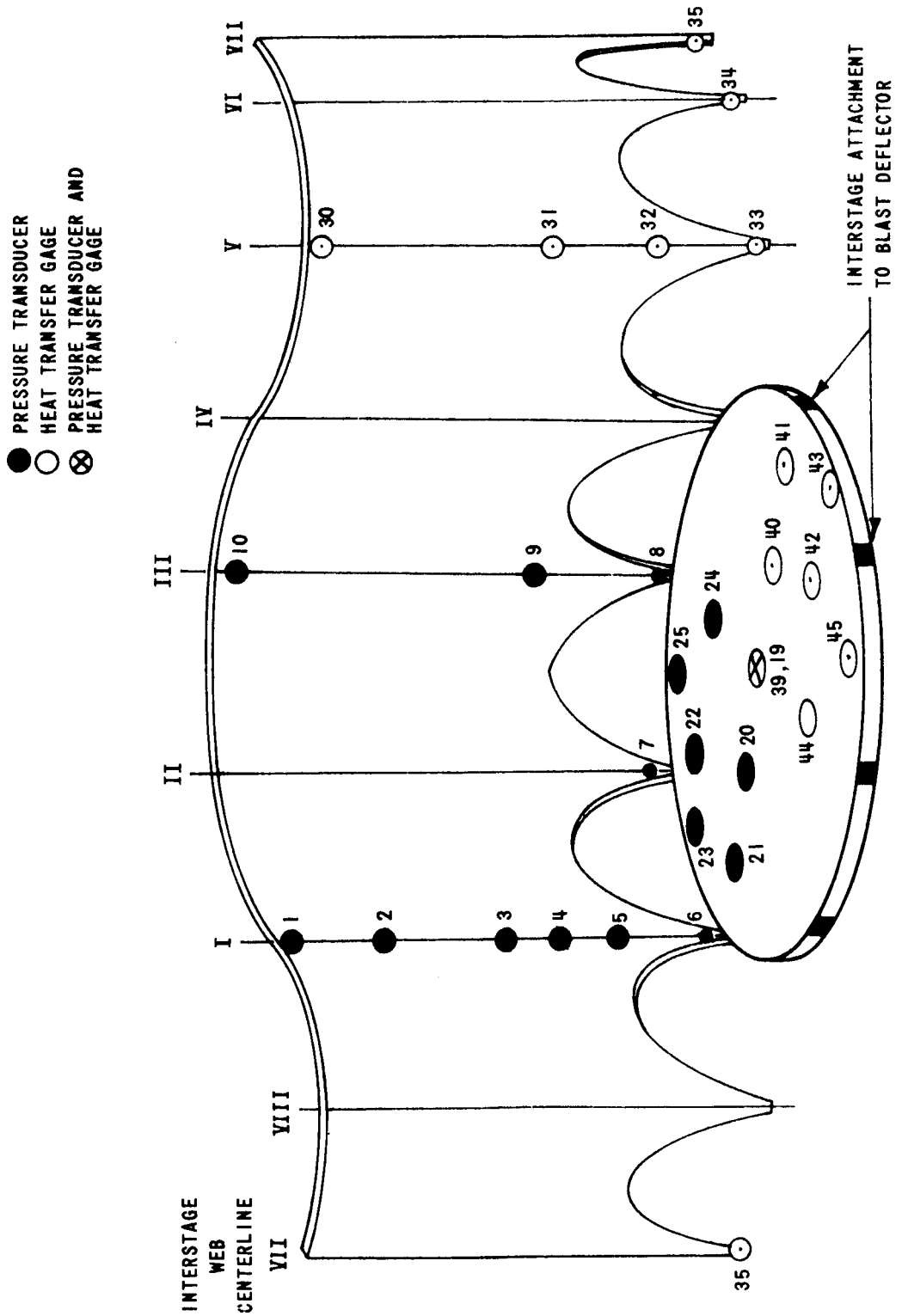

Figure 13 INTERSTAGE INSTRUMENTATION (FROM REFERENCE 8)

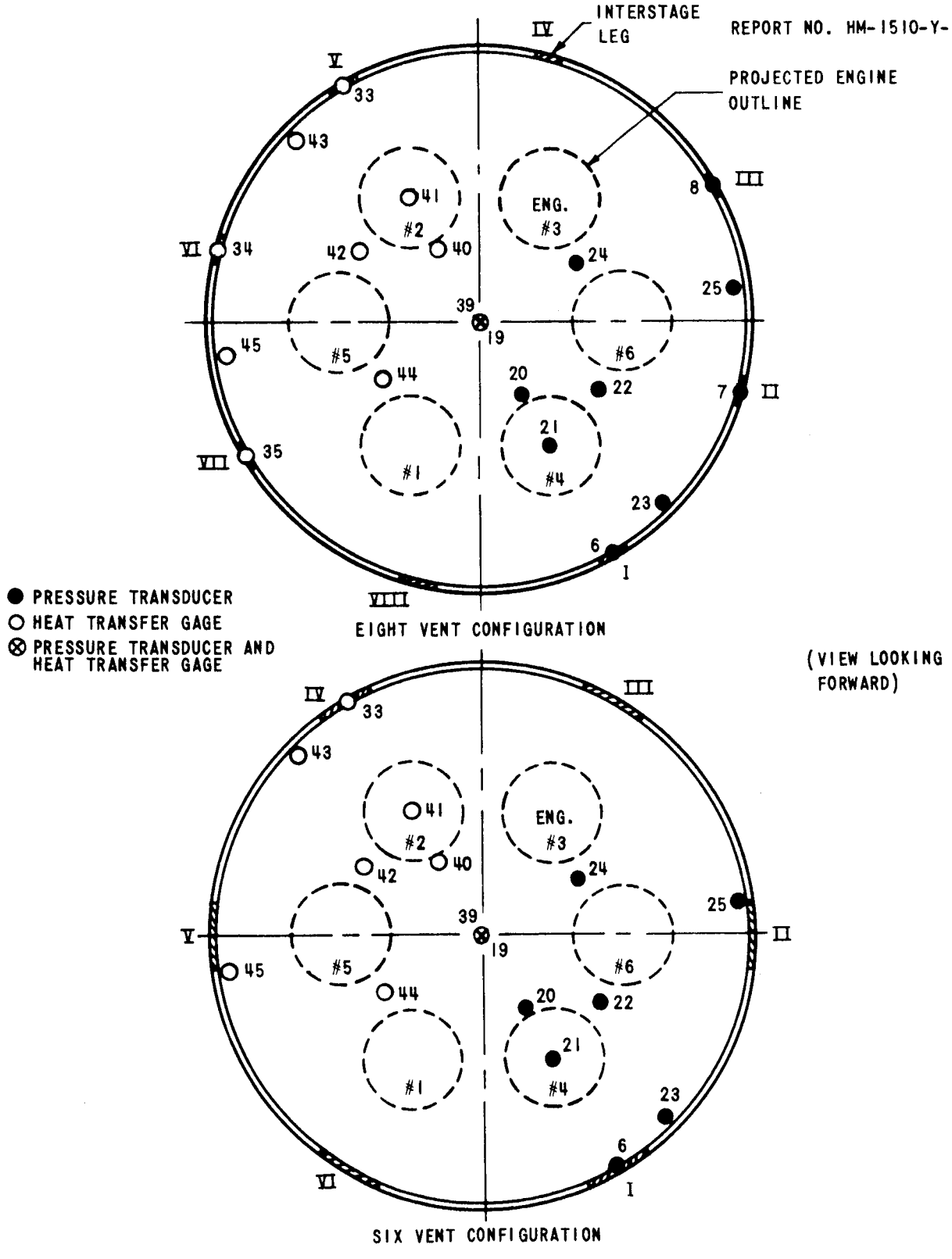

Figure 14 BLAST DEFLECTOR INSTRUMENTATION (FROM REFERENCE 8)

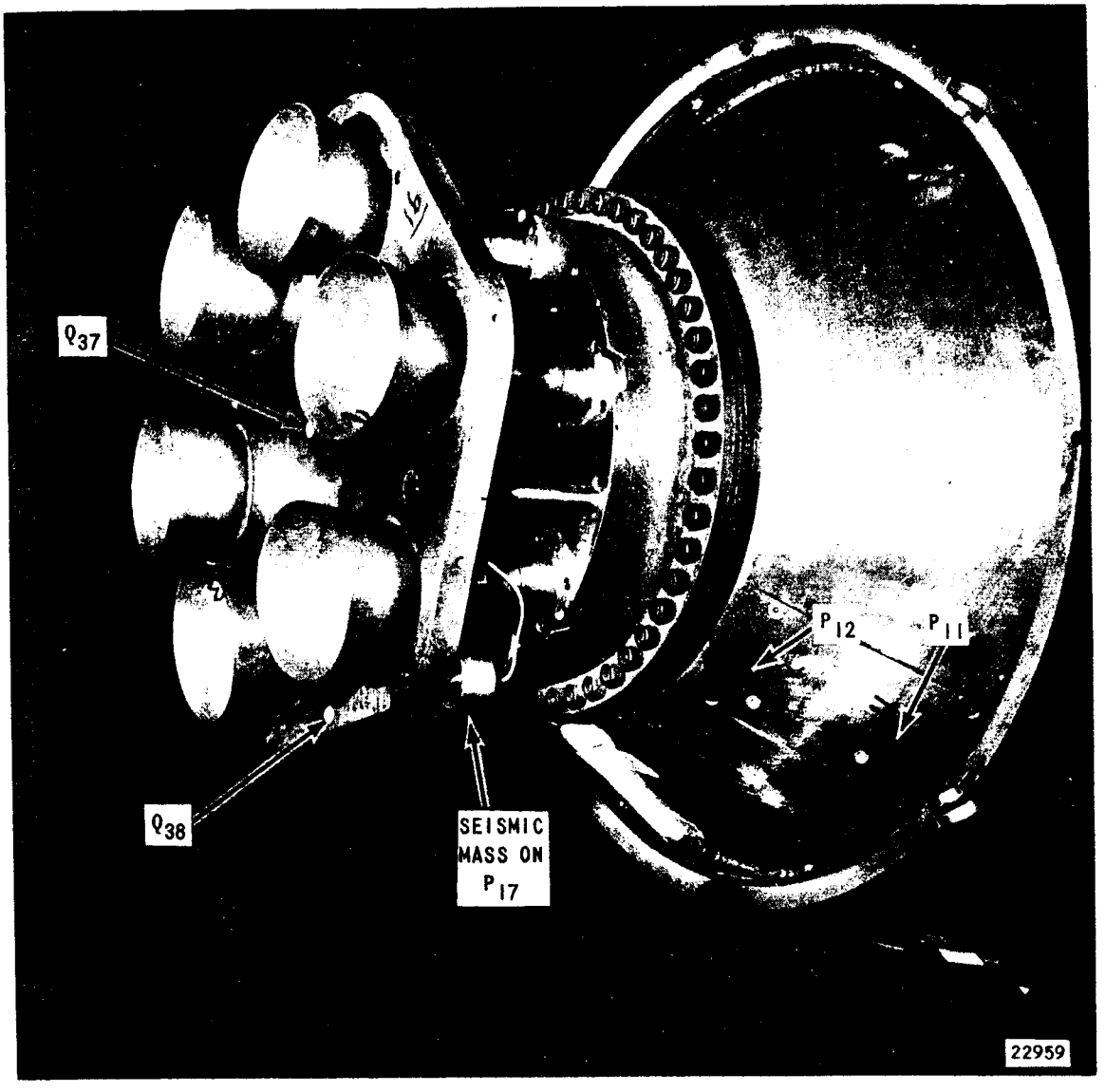

HEAT SHIELD AND THRUST STRUCTURE SHOWING SOME INSTRUMENTATION

Figure 15

BLAST DEFLECTOR AND INTERSTAGE INTERIOR SHOWING SOME INSTRUMENTATION

Figure 16

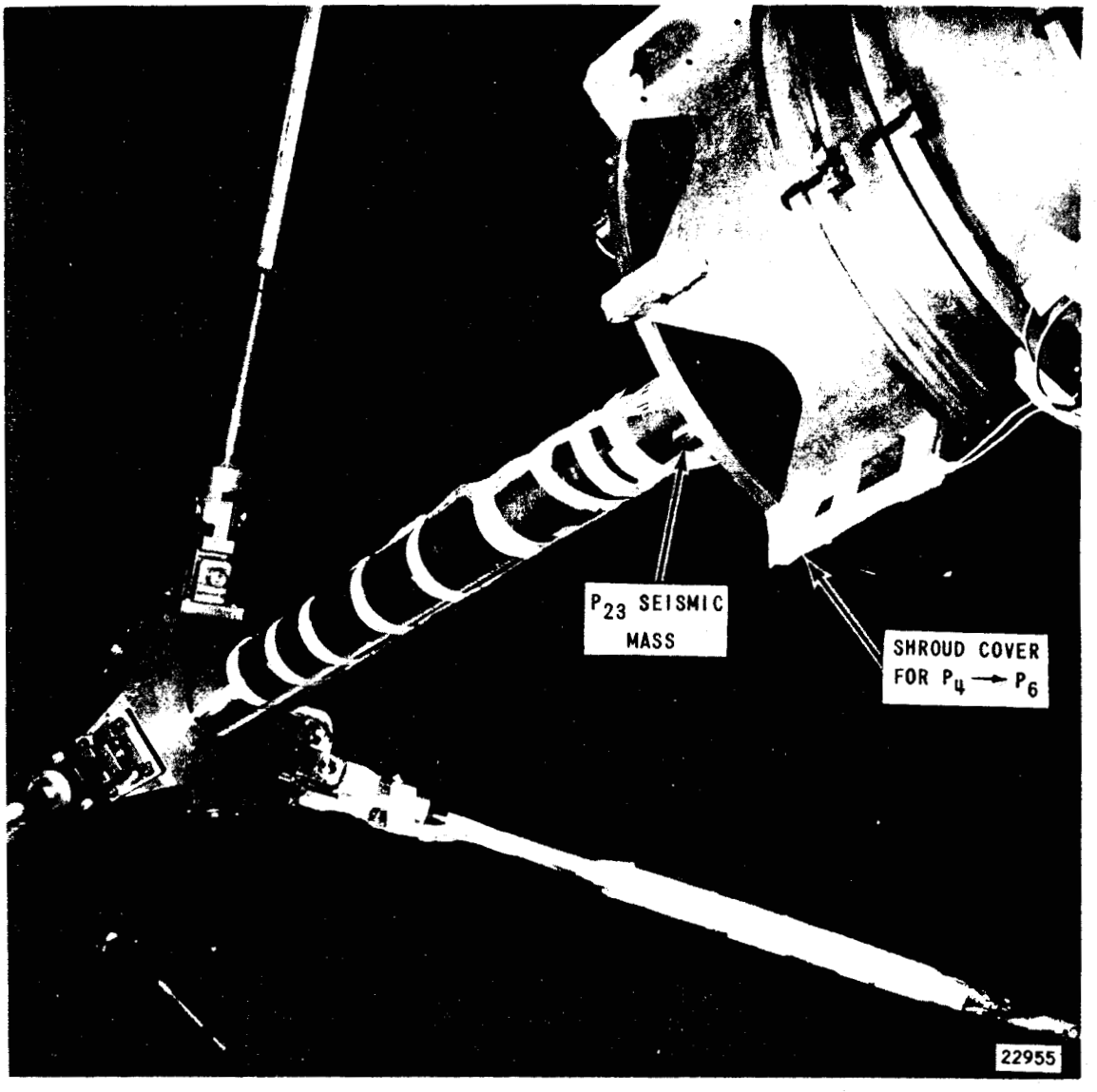

INTERSTAGE AND SUPPORT SYSTEM (LOOKING DOWNSTREAM)

Figure 17

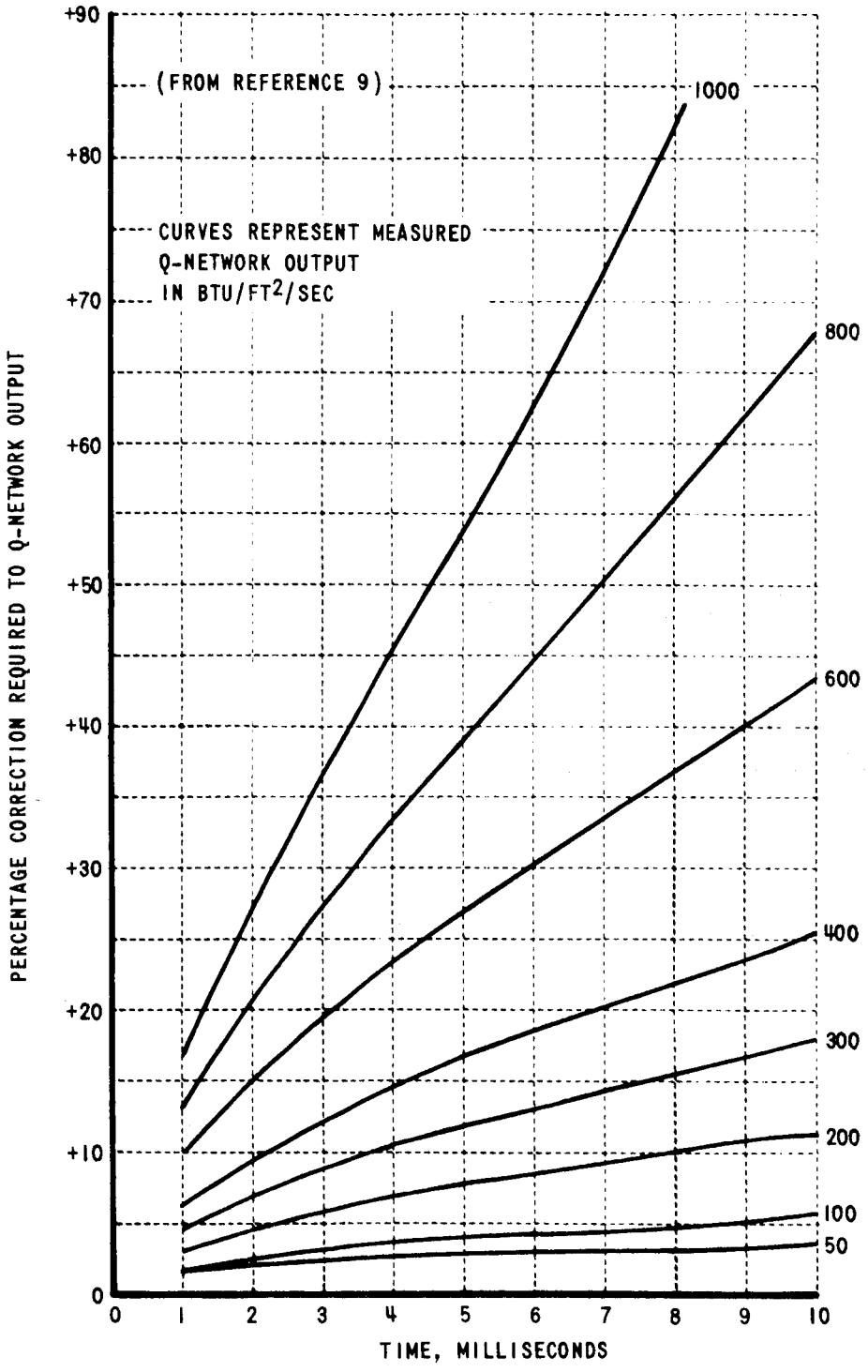

Figure 18 CORRECTIONS TO OUTPUT OF Q-NETWORK AS A FUNCTION OF Q AND TIME

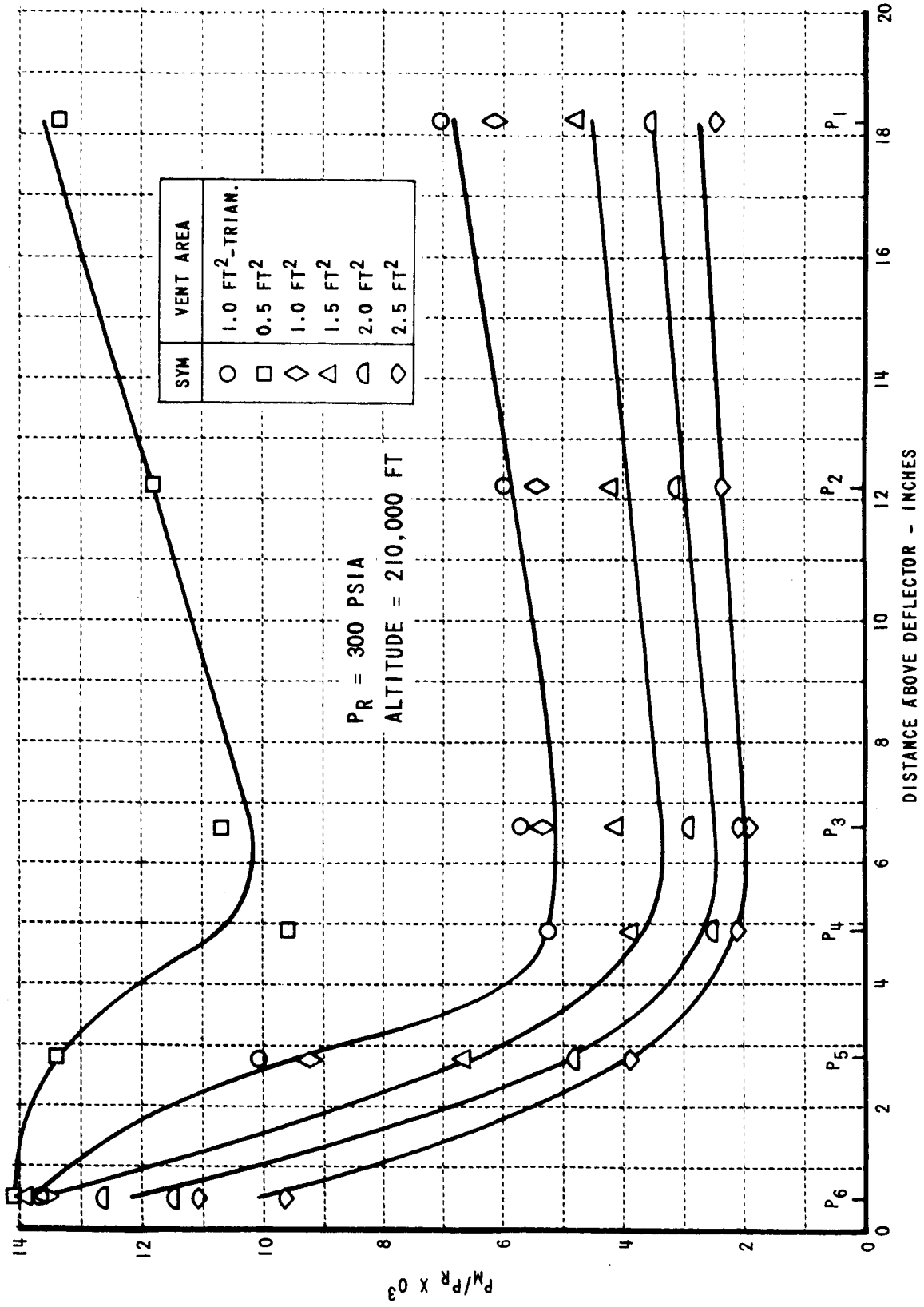

Figure 19 EFFECT OF VENT AREA ON INTERSTAGE WALL PRESSURES (ADJACENT TO AN ENGINE)

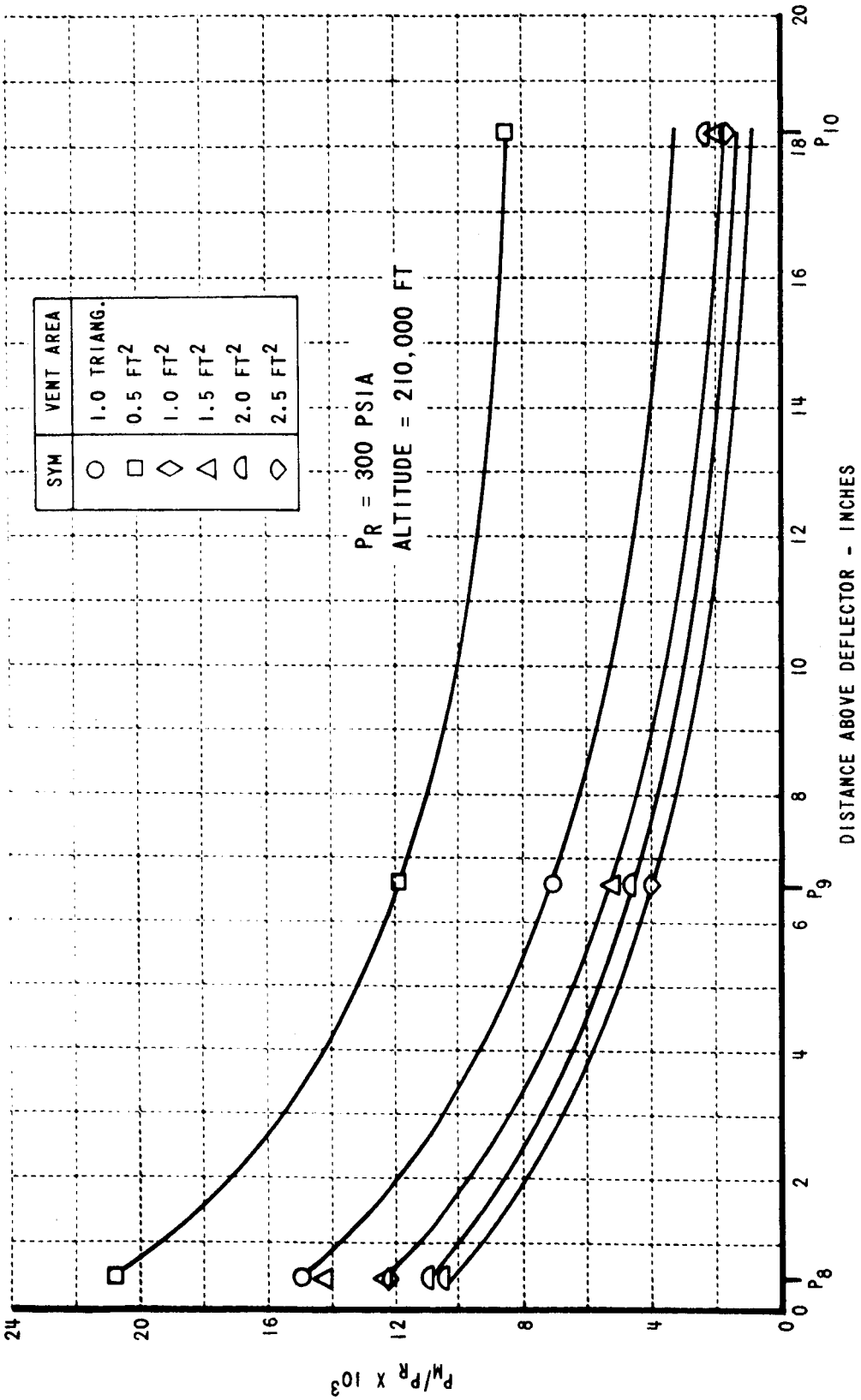

Figure 20 EFFECT OF VENT AREA ON INTERSTAGE WALL PRESSURE (BETWEEN ADJACENT ENGINES)

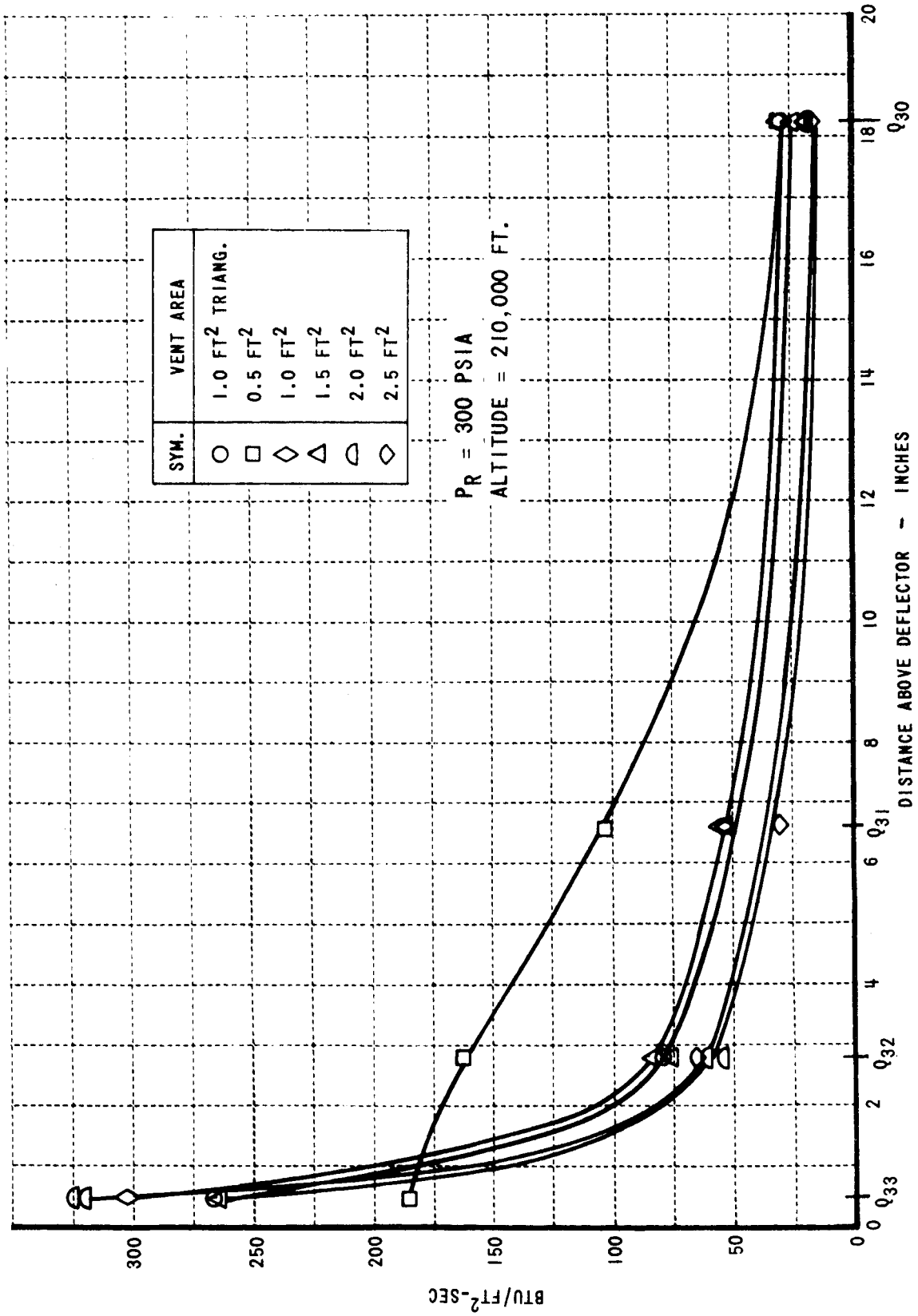

Figure 21 EFFECT OF VENT AREA ON INTERSTAGE WALL HEAT TRANSFER RATE

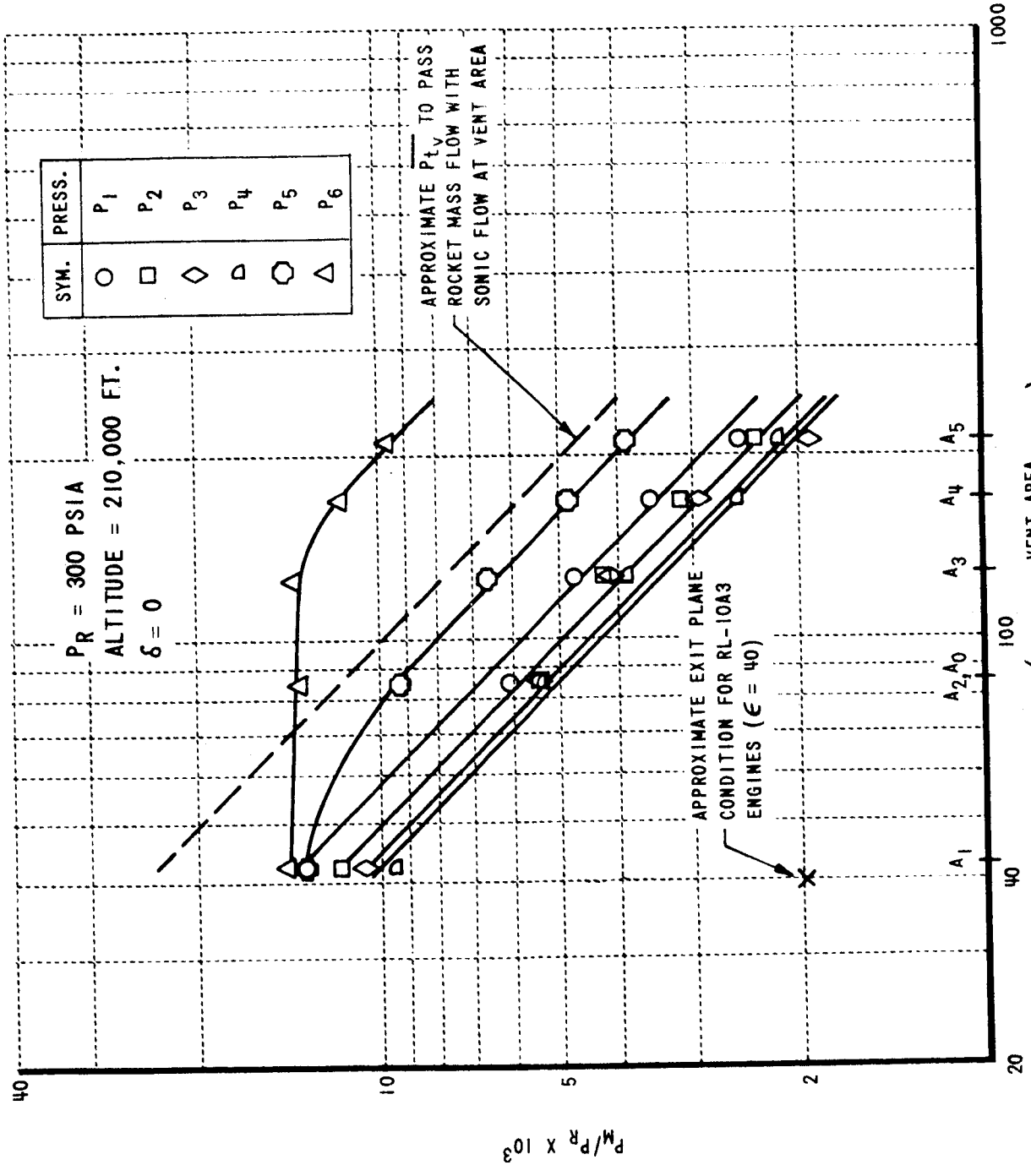

Figure 22 EFFECT OF VENT AREA ON INTERSTAGE WALL PRESSURE (ADJACENT TO AN ENGINE)

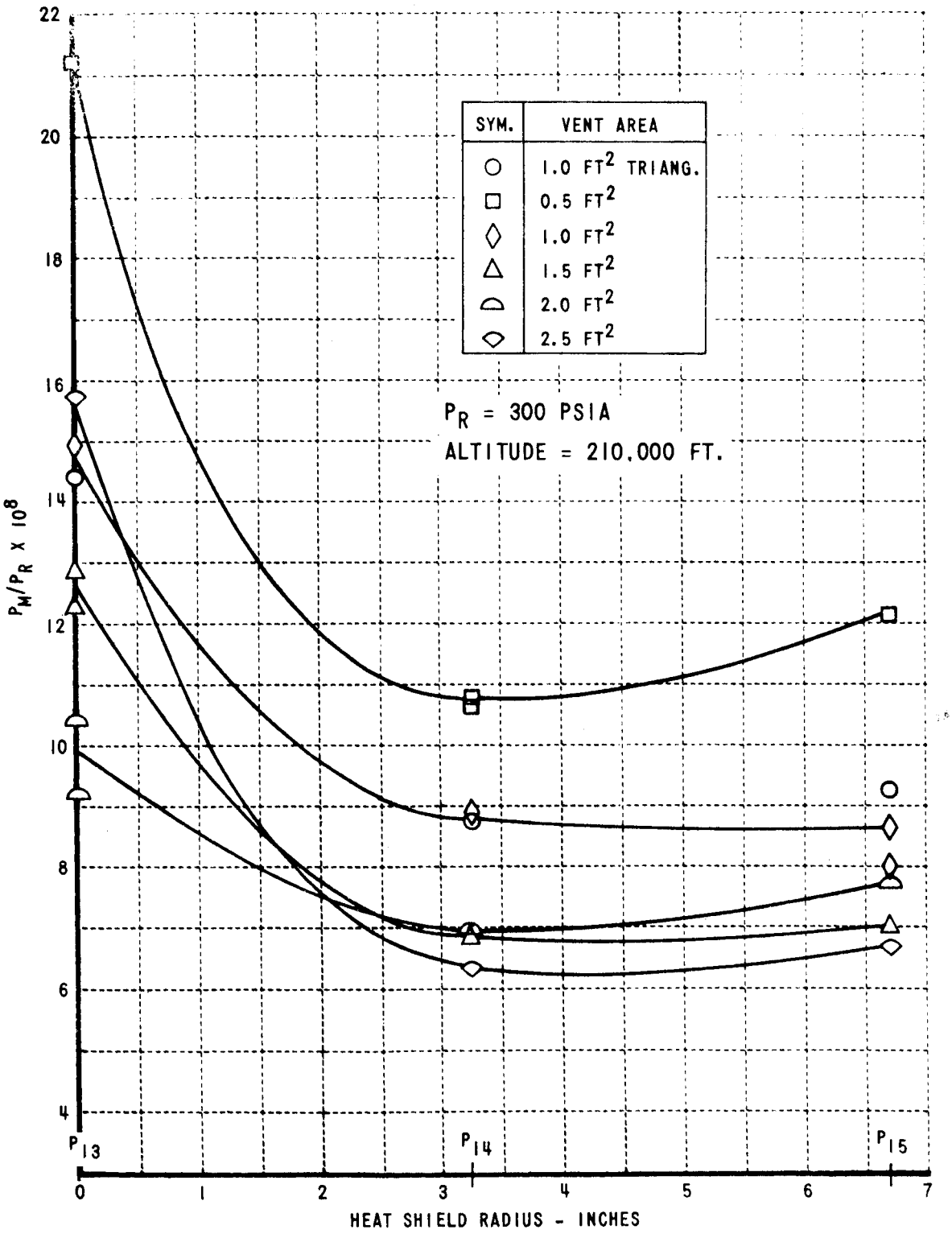

Figure 23 EFFECT OF VENT AREA ON HEAT SHIELD PRESSURES

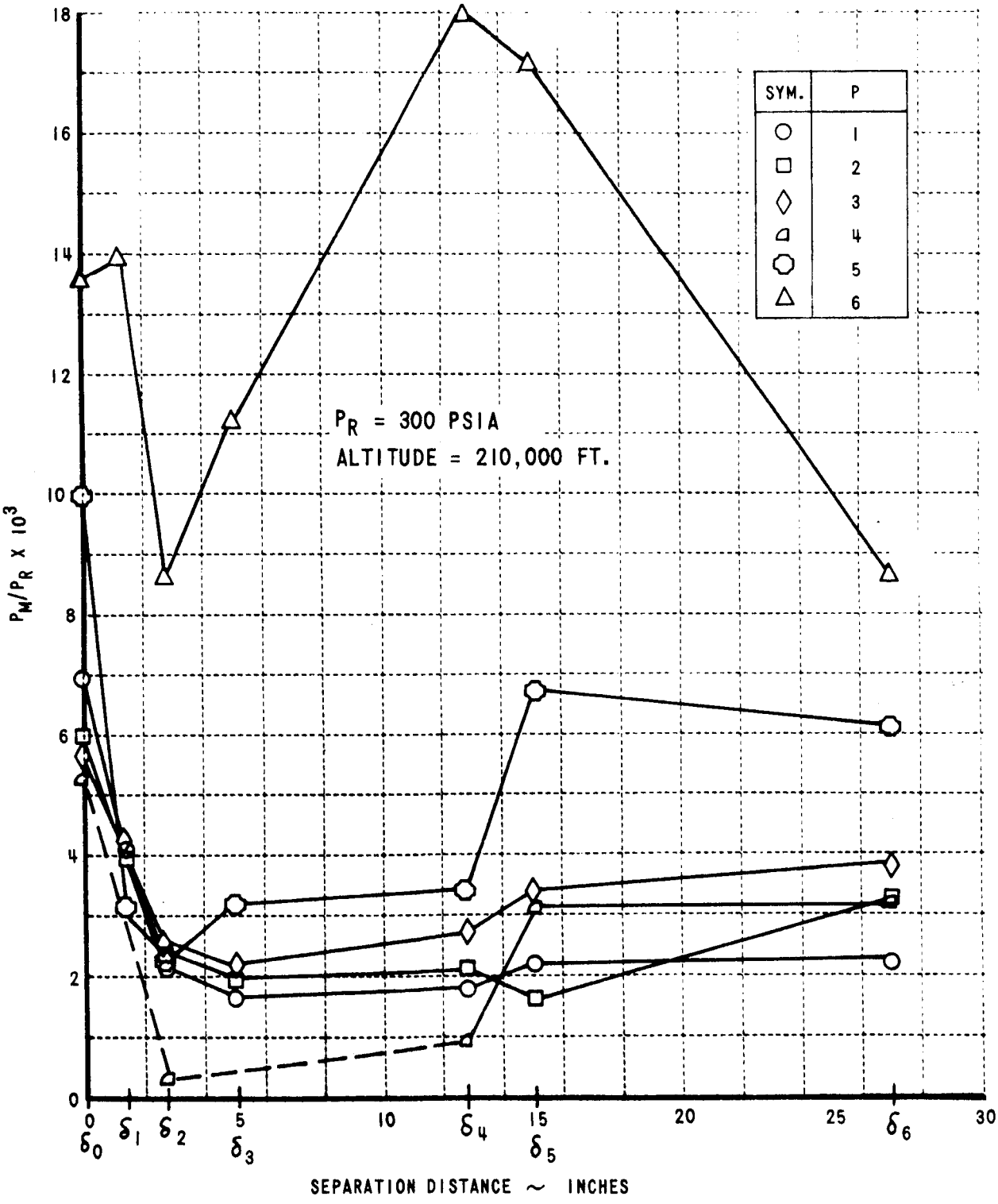

Figure 24 EFFECT OF INTERSTAGE SEPARATION DISTANCE ON INTERSTAGE WALL PRESSURES (BETWEEN ADJACENT ENGINES)-STANDARD CONFIGURATION

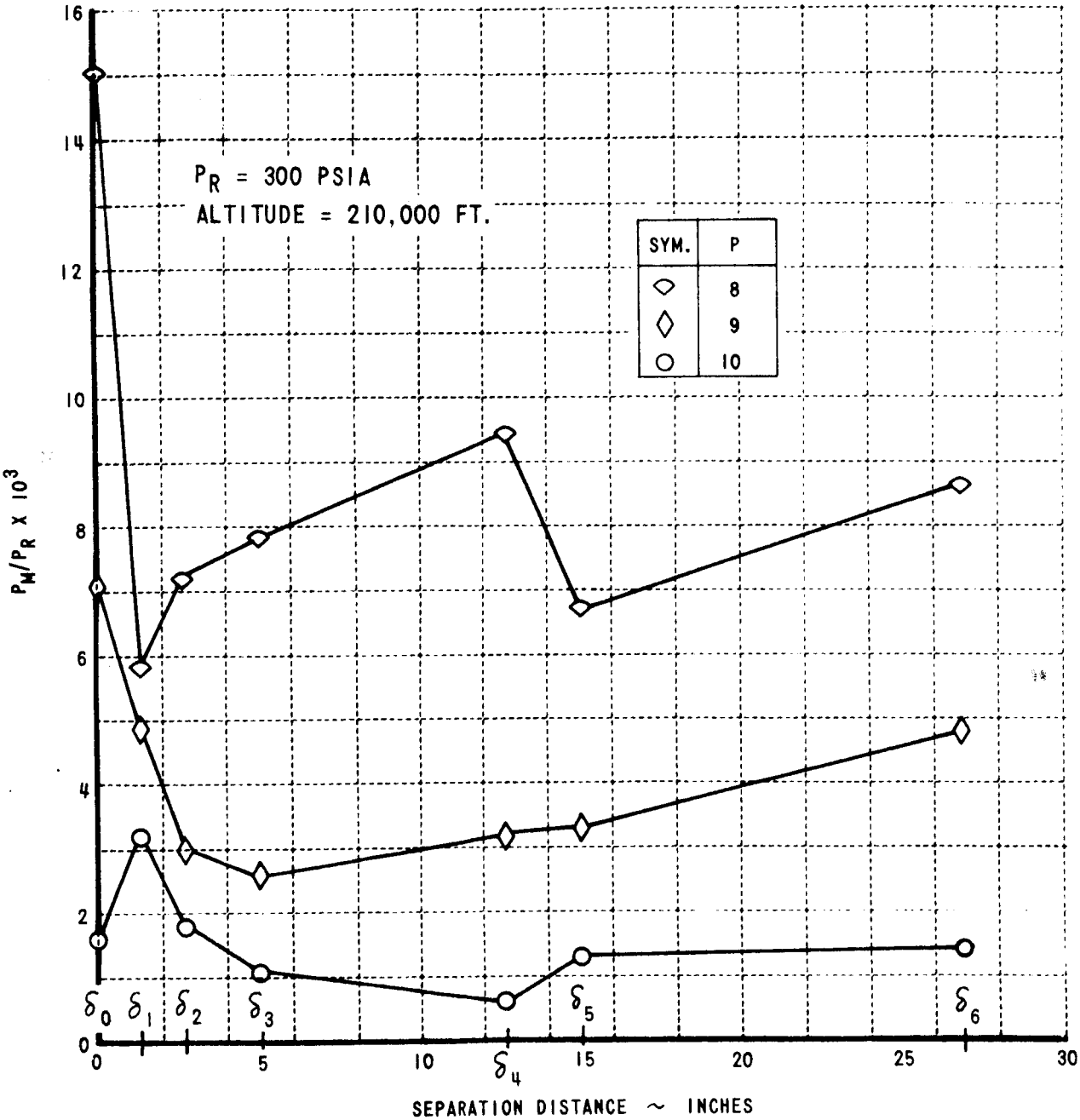

Figure 25 EFFECT OF INTERSTAGE SEPARATION DISTANCE ON INTERSTAGE WALL PRESSURES (ADJACENT TO AN ENGINE)-STANDARD CONFIGURATION

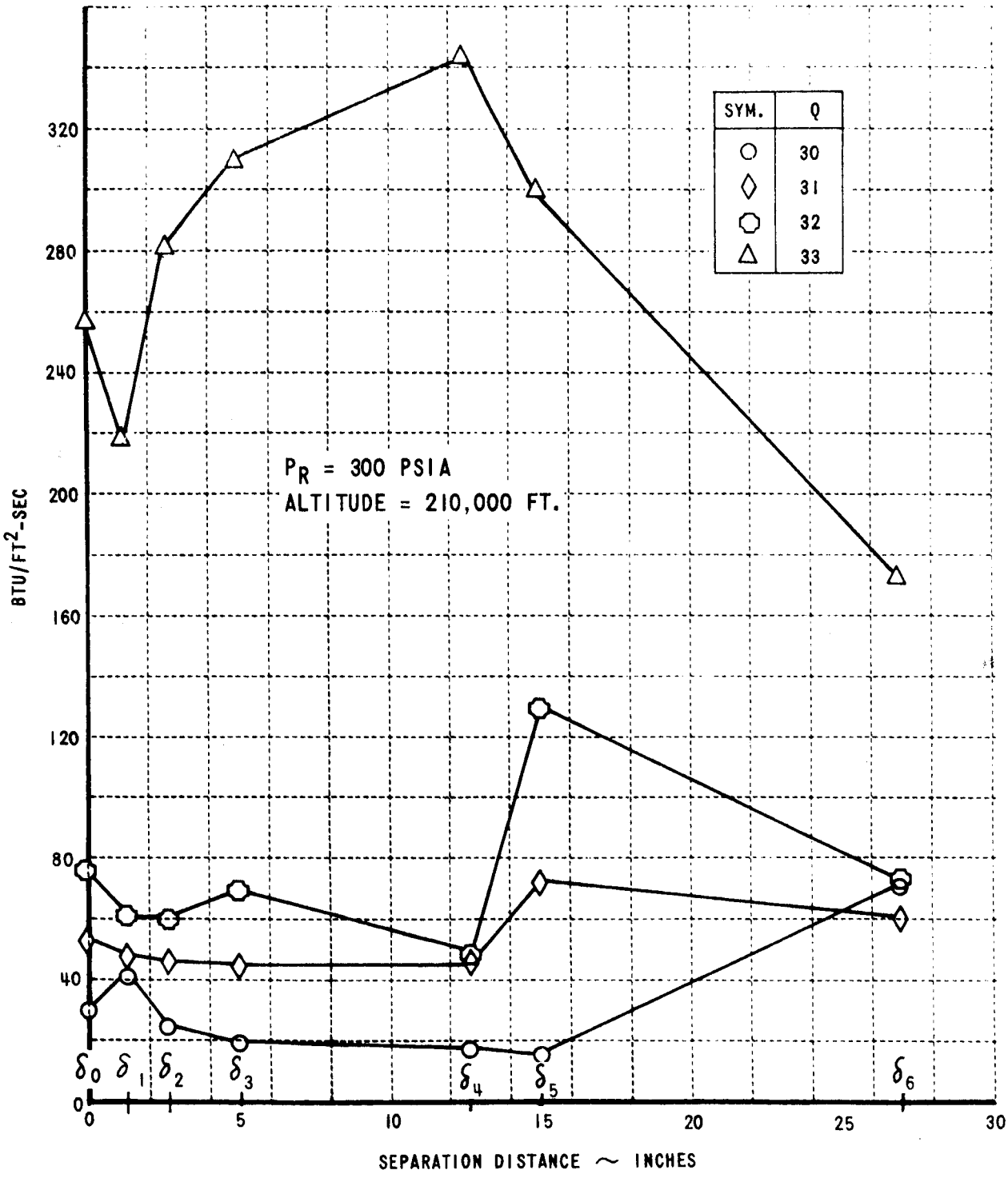

Figure 26 EFFECT OF INTERSTAGE SEPARATION DISTANCE ON INTERSTAGE WALL HEAT TRANSFER (BETWEEN ADJACENT ENGINES)-STANDARD CONFIGURATION

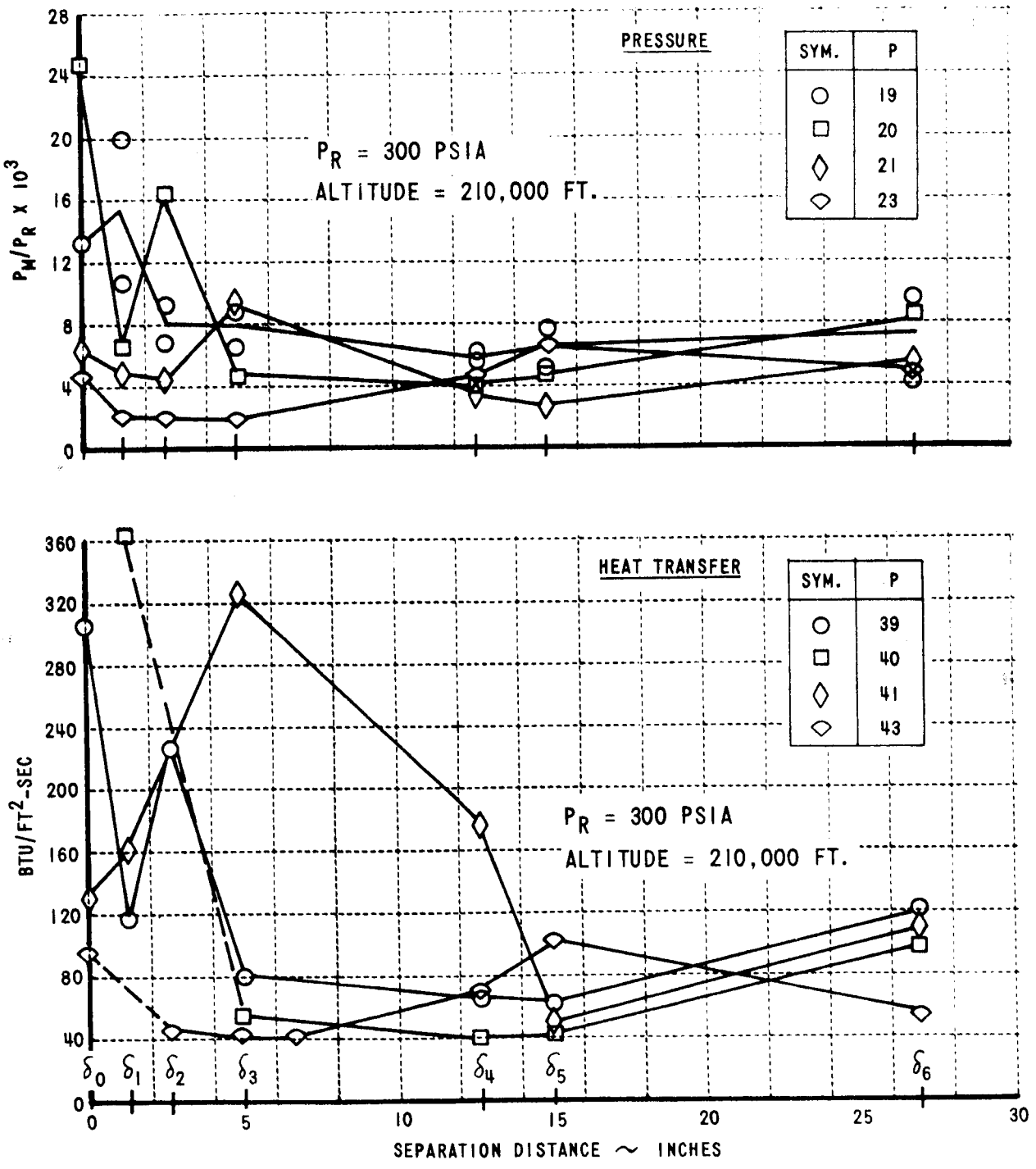

Figure 27 EFFECT OF STAGE SEPARATION DISTANCE ON BLAST DEFLECTOR PRESSURES AND HEAT TRANSFER-STANDARD CONFIGURATION

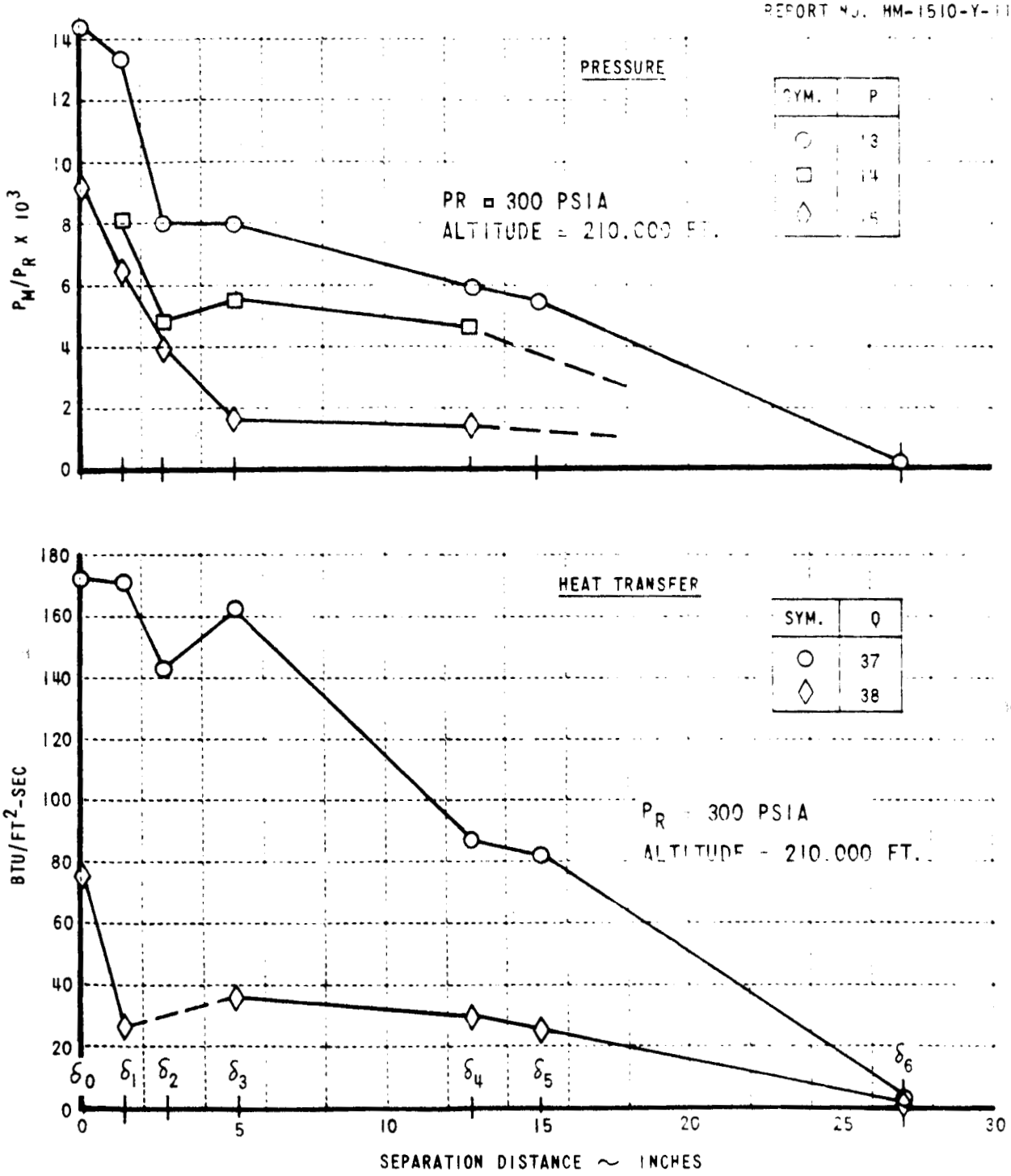

Figure 28 EFFECT OF INTERSTAGE SEPARATION DISTANCE ON HEAT SHIELD PRESSURES AND HEAT TRANSFER-STANDARD CONFIGURATION

APPENDIX A

TEMPERATURE-TIME HISTORIES FROM POST-TEST $\dot{Q}$ INVERSION

During the data analysis phase, a number of heat transfer data points were randomly selected for detailed examination. The purpose of this was twofold; i.e. 1) to determine actual gage temperatures at the time the data were read, and 2) to compare the conventional digitally computed heat transfer data with analog data appropriately corrected by the procedures of Figure 18. A knowledge of the actual gage temperature history is useful for several reasons. For instance, surface temperature, in conjunction with an estimate of the recovery temperature, will allow film coefficients to be calculated. Alternately, in cases where the surface temperature increases sufficiently during the test period to significantly reduce the temperature difference between the gas and wall ($T_R - T_W$), a knowledge of the instantaneous wall temperatures provides a basis for correcting the measured heat transfer rates to account for such effects.

Since the analog q-meter circuits had been used exclusively during the program, only heat transfer rates had been recorded and no temperature-time histories were available. It then became necessary to work "backwards" and convert the oscilloscope heat transfer records into their equivalent temperature traces. This was accomplished by means of a photoformer and inverse $\dot{q}$-network described below. The temperature-time histories subsequently determined were then reduced to heat transfer by the conventional techniques.

The photoformer derives its name from the fact that it generates wave shapes by the use of a photomultiplier tube in combination with a cathode-ray tube. An opaque mask, contoured to the desired wave shape, is attached to the face of the cathode-ray tube and a phototube is placed in a position to view the screen. The mask is generally positioned so that the lower portions of the screen are opaque and the upper portions clear. A saw-tooth voltage is applied to the horizontal deflection plates of the cathode-ray tube to generate a beam sweep linear with time. The vertical plates are driven by a suitable amplifier whose input signal is obtained from the phototube.

APPENDIX A (Cont.)

A signal will be obtained from the phototube whenever the beam strikes the screen above the opaque portions of the mask. The amplifier is so connected that whenever the phototube "sees" the beam spot, it will drive the beam downward toward the mask edge. Conversely, whenever the beam is not "seen", it will be driven upward toward the mask edge. Thus a feedback loop is established, and if the loop gain is sufficiently high, the beam-spot will be caused to accurately track the edge of the mask.

If it is assumed (a reasonable assumption in practice) that the deflection sensitivity of the cathode-ray tube is independent of beam position, then the output voltage of the amplifier is proportional to beam-spot height. Also, since the spot height is essentially the mask height, the output voltage is likewise proportional to mask height under equilibrium conditions. The time to achieve equilibrium is determined by the total time lag in the feedback loop and is comprised of response lags associated with the screen phosphor (decay time), phototube, and amplifier.

Since the horizontal beam displacement is essentially proportional to the horizontal deflection voltage and since the amplifier output voltage is proportional to the height of the mask, the output signal bears a relation to the sweep signal (time) substantially identical to the relationship between the vertical height of the mask and the horizontal distance measured along the mask. Thus, any single-valued function can be generated once a suitable mask is obtained.

The masks for the photoformer were made by replotting the original oscilloscope $\dot{q}$-network data to a suitable scale, transferring this information to a clear plastic sheet and blackening the area below the curve.

APPENDIX A (Cont.)

The inverse $\dot{q}$-network essentially solves the inverse of the equation that is solved by the $\dot{q}$-network. This equation is as follows:

$$\Delta T = \frac{2\dot{q}\sqrt{t}}{\sqrt{\pi \rho c k}}$$

where ΔT = temperature rise

$\dot{q}$ = heat transfer rate

t = time

ρ = density of gage substrate

c = specific heat of gage substrate

k = thermal conductivity of gage substrate

When consistent units are employed one can determine the time at which ΔT will be numerically equal to $\dot{q}$. Knowing this, the system is calibrated in the following manner. A mask in the form of a step is made to the same scale as the raw $\dot{q}$-data. This mask is inserted in the photoformer and the scanned signal is fed through an inverse $\dot{q}$-network producing a parabolic output. Upon solving the above equation for the time at which ΔT numerically equals $\dot{q}$, the amplitude of the parabola at that time is read, thus establishing a calibration for the temperature trace.

Typical time histories of temperature and heat transfer rate are shown in Figures A-1 and A-2. A comparison of the appropriately corrected data read directly from the $\dot{q}$-meter is shown at several times by the solid symbols.

Although the quantitative agreement between directly measured $\dot{q}$-meter data and the $\dot{q}$-data from the inverse $\dot{q}$-network and digital program is not exact, there is a noticeable qualitative agreement. Quantitative differences of the order of five percent are observed. This agreement is considered excellent since numerous possibilities exist for errors to enter the system in the process of converting the original analog $\dot{q}$-data to equivalent temperature histories.

APPENDIX A (Cont.)

These errors can be introduced through mask reproduction, scaling factors, inverse $\dot{q}$-network/photoformer equipment instabilities, and other sources.

The relationship between $\dot{q}$ and ΔT at times approaching the test interval can also be noted from Figures A-1 and A-2. In general, $\dot{q}$ is numerically equal to ΔT at about 5-7 ms. Thus, at the time for which the analog $\dot{q}$-data was read in the test program data reduction, the corresponding gage temperature (in °F) will be on the order of 10-20 percent greater than the numerical value of $\dot{q}$ (in Btu/ft^2-sec) reported herein.

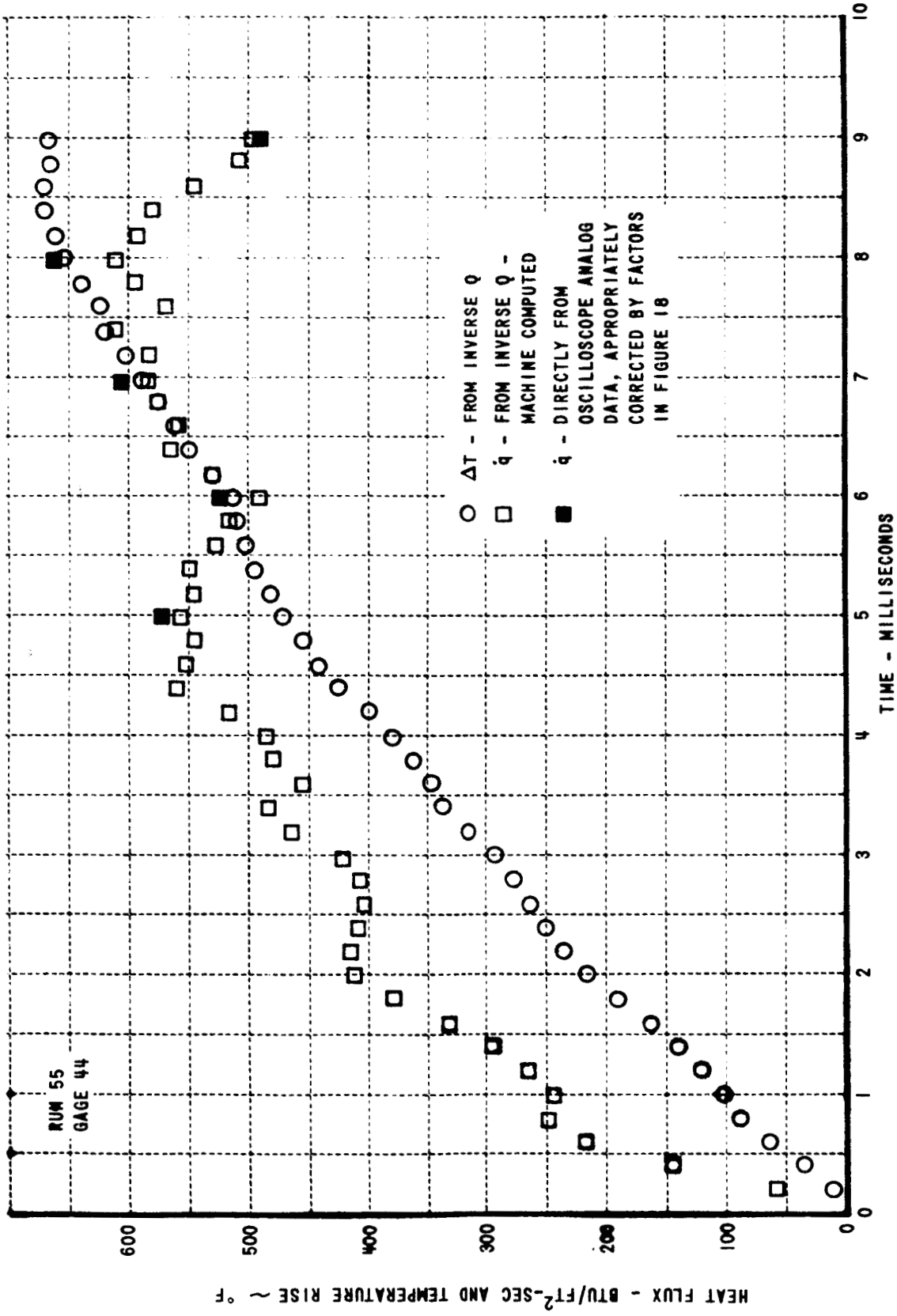

Figure A-1 TYPICAL TEMPERATURE/HEAT FLUX TIME HISTORIES

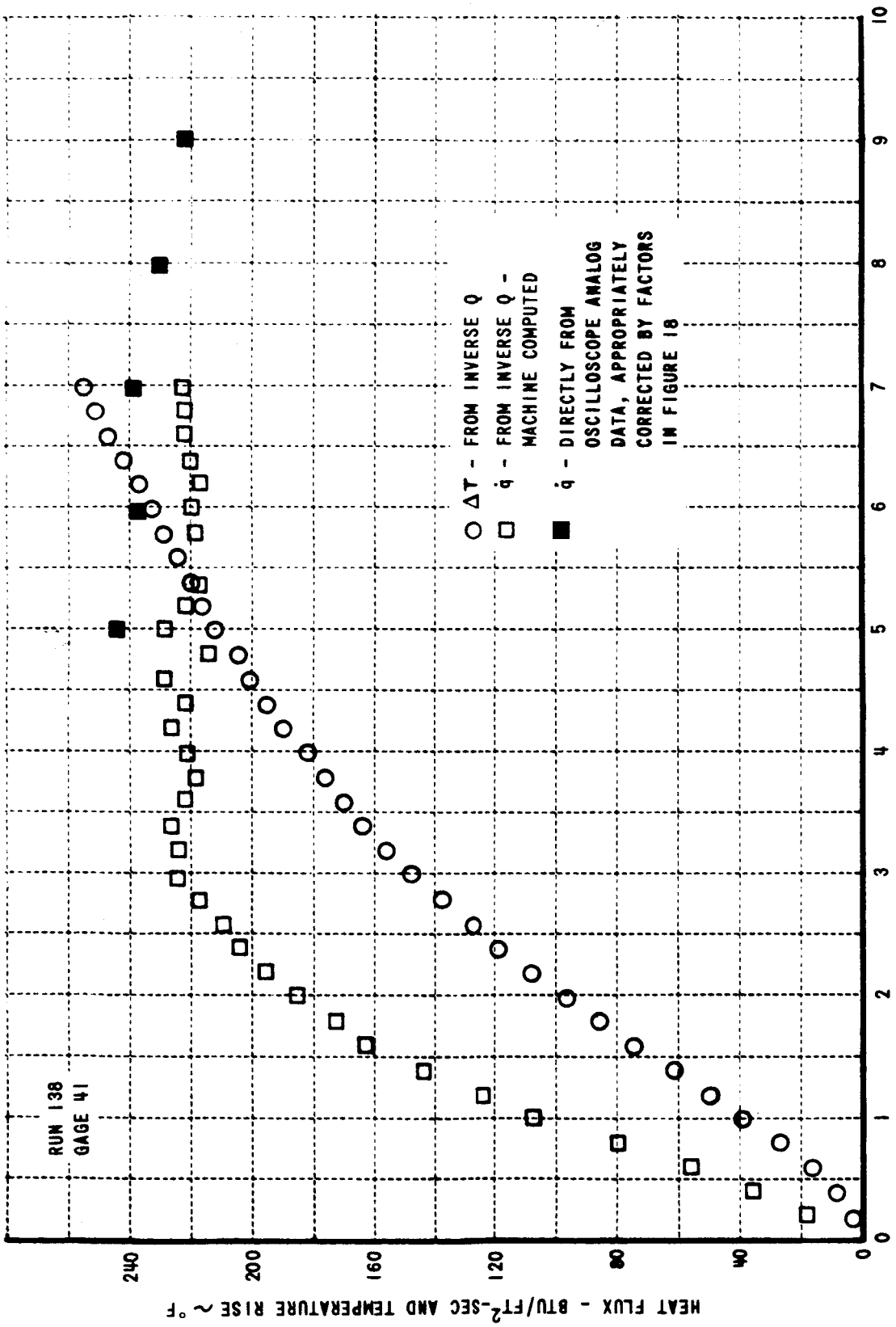

Figure A-2 TYPICAL TEMPERATURE/HEAT FLUX HISTORIES